A study on the structural behaviour of functionally graded porous plates on elastic foundation using a new quasi-3D model: Bending and free vibration analysis

Miloud Kaddari[1], Abdelhakim Kaci[*1,2,3], Abdelmoumen Anis Bousahla[2,4], Abdelouahed Tounsi[1,2], Fouad Bourada[1,2,5], AbdeldjebbarTounsi[1,2], E.A. Adda Bedia[2] and Mohammed A. Al-Osta[2]

[1]*Material and Hydrology Laboratory, University of Sidi Bel Abbes, Faculty of Technology, Civil Engineering Department, Algeria*
[2]*Department of Civil and Environmental Engineering, King Fahd University of Petroleum & Minerals, 31261 Dhahran, Eastern Province, Saudi Arabia*
[3]*Department of Civil Engineering and Hydraulics, University Dr. Taher Moulay of Saida, Algeria*
[4]*Laboratoire de Modélisation et Simulation Multi-échelle, Département de Physique, Faculté des Sciences Exactes, Département de Physique, Université de Sidi Bel Abbés, Algeria*
[5]*Département des Sciences et de la Technologie, Centre Universitaire de Tissemsilt, BP 38004 Ben Hamouda, Algeria*

Abstract. This work investigates a new type of quasi-3D hyperbolic shear deformation theory is proposed in this study to discuss the statics and free vibration of functionally graded porous plates resting on elastic foundations. Material properties of porous FG plate are defined by rule of the mixture with an additional term of porosity in the through-thickness direction. By including indeterminate integral variables, the number of unknowns and governing equations of the present theory is reduced, and therefore, it is easy to use. The present approach to plate theory takes into account both transverse shear and normal deformations and satisfies the boundary conditions of zero tensile stress on the plate surfaces. The equations of motion are derived from the Hamilton principle. Analytical solutions are obtained for a simply supported plate. Contrary to any other theory, the number of unknown functions involved in the displacement field is only five, as compared to six or more in the case of other shear and normal deformation theories. A comparison with the corresponding results is made to verify the accuracy and efficiency of the present theory. The influences of the porosity parameter, power-law index, aspect ratio, thickness ratio and the foundation parameters on bending and vibration of porous FG plate.

Keywords: static; free vibration; novel Quasi-3D plate theory; normal stress; porous FG; Kerr foundation

1. Introduction

Functionally graded materials (FGMs) are a class of composites in which the properties of materials vary continuously from one point to another. This is achieved by varying the volume fraction of the constituents, for example ceramic and metal, in a predetermined manner. This constantly changing composition eliminates interface problems and, as a result, the stress distribution is smooth. Over the last few years, FGMs are now developed for general use as structural elements in different applications. The reason for the increasing use of FGMs in various aerospace, automotive, civil and mechanical structures is that their material properties can be adapted to different applications and work environments. The evidence is the very big amount of literature on these materials (Qian and Batra 2005, Darlmaz 2015, Ebrahimi and Dashti 2015, Bouguenina *et al*. 2015, Akbas 2015, Arefi 2015, Pradhan and Chakraverty 2015, Kar and Panda 2015, Ebrahimi and Habibi 2016, Moradi-Dastjerdi 2016, Laoufi *et al*. 2016).

As a result, various theories have been developed by researchers to predict the good bending behavior of FGM material plates. Kirchhoff has developed a classical plate theory (CPT) for thin plate analysis, which is based on the Kirchhoff hypothesis where transverse shear deformations are zero and therefore transversal stresses do not enter the theory. This theory does not include shear effects and therefore only applies to thin plates (Abrate 2008, Arefi 2015, Pradhan 2015, Darilmaz 2015). Conventional plate theory will give erroneous results when used for thick plates (Liu 2011).

To account for the transverse shear stress, Reissner (Reissner 1945) and Mindlin (Mindlin 1951) developed a first order shear deformation plate theory (FSDT) by considering the effect of transverse shear deformation for analysis the plates. In this theory the basic equations are derived by assumption that the in-plane displacements are linearly distributed across the plate thickness. This leads to constant transverse shear stresses over the entire thickness of the plate, so that the condition of zero shear stress on the face of the plate is not satisfied and requires a shear correction factor difficult to find because it depends on the geometries, the material properties and the boundary conditions of each problem (Ferreira *et al*. 2009).

Following the limitations of the CPT and FSDT

---

*Corresponding author, Professor
E-mail: kaci_abdelhakim@yahoo.fr

theories, a significant number of higher order shear deformation plate theories (HSDT) that do not require a shear correction factor and satisfy zero shear stress conditions on the upper and lower surfaces of the plates have been developed and this, to correctly approximate the nonlinear distribution of transverse shear deformations along the thickness of the plate (Bensaid 2017, Belkacem *et al.* 2018, Karami and Janghorban 2019).

Often 2-D plate theories mentioned above (CPT, FSDT and HSDT, and RHSDTs) overlook the influence of thickness stretching effect (i.e., $\varepsilon_z = 0$) due to assuming constant transverse displacements through the thickness. Recently, many quasi-3D theories have been proposed in the literature where the effect of thickness stretching (ε_z) in FG plates was investigated by different investigators (Akavci and Tanrikulu 2015, Adim and Daouadji 2016, Kar and Panda 2016, Hadji *et al.* 2018) to reach accurate results. It should be noted also that experimental study are conducted together with HSDTs to investigate the mechanical behaviors of structures (Sahoo *et al.* 2016, Hirwani *et al.* 2016a, 2018a, b, c, Mehar *et al.* 2017, Sahoo *et al.* 2017a, b, 2018, Hirwani and Panda 2018, Chandra Mouli *et al.* 2018, Bisen *et al.* 2018, Mehar and Panda 2018 and 2019, Pandey *et al.* 2019, Sahoo *et al.* 2019, Mehar *et al.* 2019).

These theories which looks like higher-order theory uses only five unknown functions in order to derive five governing equations for functionally graded plates. The thickness stretching effect becomes very valuable for thick plates analysis and hence has to be taken into consideration. Many quasi-3D theories have been proposed in the literature (Thai and Kim 2013, Thai *et al.* 2014, Neves *et al.* 2012, Neves *et al.* 2013). Thai and Kim (2012) proposed a simple quasi-3D sinusoidal-shear-deformation theory to analyze the bending behavior of FG plates by utilizing five unknown variables. Bourada *et al.* (2015) proposed a new simple shear and normal deformations theory for functionally graded beams. A refined plate theory was developed to account for the thickness stretching effect in functionally graded plates by Thai *et al.* (2012).

With the rapid advancement in technology of structure components, structures with graded porosity can be considered as one of the latest developments in FGMs. For example, Amar *et al.* (2017) presented a new hyperbolic shear deformation beam theory is proposed based on a modified couple stress theory (MCST) to investigate the bending and free vibration responses of functionally graded (FG) micro beam made of porous material. Ehyaei *et al.* (2017) studied the effect of porosity and axial preload on vibration behavior of rotating FG nanobeam. Zenkour (2018) presented a quasi-3D refined theory for functionally graded single-layered and sandwich plates with porosities. Faleh *et al.* (2018) investigated the vibration response of porous FG nanoshells. Salari *et al.* (2019) examined the porosity-dependent asymmetric thermal buckling of inhomogeneous annular nanoplates resting on elastic substrate. Avcar (2019) studied recently the free vibration of imperfect sigmoid and power law functionally graded beams.

The interaction action between structures and supporting soil media is of fundamental importance in foundation design and it has always attracted the attention of both researchers and engineers. There are many studies on elastic foundation modeling Winkler in literature. This is the simplest model was introduced by Winkler in 1867 known as the one-parameter model concerning the elastic base, which considers the base as a series of separate springs without mating effects. This was later improved by Pasternak who took into account the interactions between the separate springs. Therefore, the Pasternak model was widely used for describe the mechanical behavior of elastic structure-base interactions (Pasternak 1954). As a generalization of the Pasternak concept, Kerr (1964) proposed a three-parameter foundation model that consists of two layers of elastic springs interconnected by an elastic shear layer.

This work aims to develop a simple quasi-3D theory with just five unknown displacement functions are used in the present theory against six or more unknown displacement functions used in the corresponding ones for analyzed bending and free vibration analysis of FG plates with graded porosity can be considered as one of the latest developments in FGMs embedded within elastic foundation. The effects due to transverse shear and normal deformations are both included. Analytical solutions are obtained for FG plate, and its accuracy of the Winkler, Pasternak and Kerr models measured against the elastic continuum model is verified by comparing the obtained results with those reported in the literature.

2. Constitutive relations

Assume that the FG plate is made of a mixture of metal and ceramic, the material properties of the plate like the Young's modulus E, the mass density ρ and Poisson's ratio v are considered to change continuously through the thickness according to a distribution power law. However, the influence of porosities, which may exist inside the FG plate materials during production, is included. The modified rule of mixtures for the two-phase FG plate with even porosities can be expressed as (Amar *et al.* 2017, Wattanasakulpong and Ungbhakorn 2014, Benferhat *et al.* 2016).

$$P(z) = P_c\left(V_c - \frac{\alpha}{2}\right) + P_m\left(V_m - \frac{\alpha}{2}\right) \qquad (1)$$

Where α is the volume fraction of porosity ($\alpha \ll 1$), for perfect FGM, α is set to zero, P_c and P_m are the material properties of ceramic and metal and V_c and V_m are the volume fraction of ceramic and metal respectively; the compositions are represented in relation to

$$V_c + V_m = 1 \qquad (2)$$

The material properties of imperfect FG plate with even porosities FGM-I can be rewritten as follow

$$E(z) = \left(E_c - E_m\right)V_c + E_m - \frac{\alpha}{2}\left(E_c + E_m\right) \qquad (3a)$$

$$\rho(z) = \left(\rho_c - \rho_m\right)V_c + \rho_m - \frac{\alpha}{2}\left(\rho_c + \rho_m\right) \qquad (3b)$$
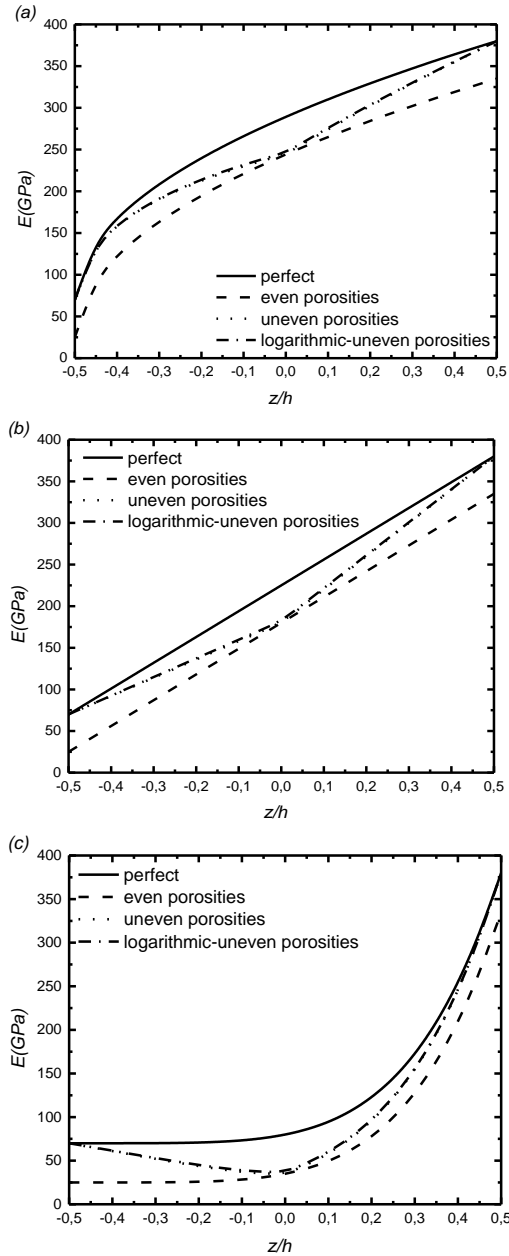
Fig. 1 variations of Young's modulus of perfect FGM and porous FGM with the thickness coordinate: (a) p=0.5; (b) p=1; (c) p=5

where $V_c = (0.5 + z/h)^p$ is the volume fraction of ceramic.

For FGM-II defined as uneven distribution model, the properties of the actual materials are in the following form as follow (Wattanasakulpong and Ungbhakorn 2014)

$$E(z) = \left(E_c - E_m\right)V_c + E_m - \frac{\alpha}{2}\left(E_c + E_m\right)\left(1 - \frac{2|z|}{h}\right) \quad (4a)$$

$$\rho(z) = \left(\rho_c - \rho_m\right)V_c + \rho_m - \frac{\alpha}{2}\left(\rho_c + \rho_m\right)\left(1 - \frac{2|z|}{h}\right) \quad (4b)$$

For FGM-III defined as uneven distribution model expanded with a logarithmic function is expanded for porosities distribution as follow

$$E(z) = \left(E_c - E_m\right)V_c + E_m - \log\left(1 + \frac{\alpha}{2}\right)\left(E_c + E_m\right)\left(1 - \frac{2|z|}{h}\right) \quad (5a)$$

$$\rho(z) = \left(\rho_c - \rho_m\right)V_c + \rho_m - \log\left(1 + \frac{\alpha}{2}\right)\left(\rho_c + \rho_m\right)\left(1 - \frac{2|z|}{h}\right) \quad (5b)$$

Fig. 1 shows the through-the-thickness variation of the Young's modulus for different power-law indexes and the porosity volume fraction is set as α=0.2. It is observed that the perfect FGM has the highest Young's modulus while the even porosities FGM-I are smallest. The Young modulus of uneven porosities FGM-II and FGM-III model expanded with a logarithmic function is between those of perfect FGM and even porosities FGM-I. In addition, the Young's modulus of FGM for uneven porosities FGM-II and III has discontinuous characteristics; it coincides with that of FGM porosity-I at the median surface of the plate and coincides with that of the perfect FGM at the upper and underlying surface of the plate, respectively.

3. Theoretical formulation

3.1 Kinematic relations and constitutive relations

The present indeterminate integral variables plate theory used by Amar *et al*. (2018) where the number of unknowns and governing equations of the present theory is reduced, and therefore, it is easy to use. The theory presented is variationally consistent, does not require shear correction factor, and gives rise to transverse shear stress variation such that the transverse shear stresses vary parabolically across the thickness satisfying shear stress free surface conditions.

$$u(x, y, z) = u_0(x, y) - z\frac{\partial w_0}{\partial x} + k_1 f(z)\int \theta(x, y)\,dx \quad (6a)$$

$$v(x, y, z) = v_0(x, y) - z\frac{\partial w_0}{\partial y} + k_2 f(z)\int \theta(x, y)\,dy \quad (6b)$$

$$w(x, y, z) = w_0(x, y) + g(z)\varphi_z \quad (6c)$$

The coefficients k_1 and k_2 depend on the geometry. where $(u_0, v_0, w_0, \theta, \varphi_z)$ are five unknown displacements of the mid-plane of the plate; and h is the plate thickness. In this study, $f(z)$ is a hyperbolic shape function chosen in the form (Ukanovic *et al*. 2018)

$$f(z) = z\left(\cosh\left(\frac{z}{h}\right) - 1.388\right) \quad (7)$$

and $g(z)$ is given as follows

$$g(z) = f'(z) \quad (8)$$

The nonzero linear strains are

$$\begin{Bmatrix} \varepsilon_x \\ \varepsilon_y \\ \gamma_{xy} \end{Bmatrix} = \begin{Bmatrix} \varepsilon_x^o \\ \varepsilon_y^o \\ \gamma_{xy}^o \end{Bmatrix} + z\begin{Bmatrix} k_x^b \\ k_y^b \\ k_{xy}^b \end{Bmatrix} + f(z)\begin{Bmatrix} k_x^s \\ k_y^s \\ k_{xy}^s \end{Bmatrix} \quad (9a)$$

$$\begin{Bmatrix} \gamma_{yz} \\ \gamma_{xz} \end{Bmatrix} = g(z) \begin{Bmatrix} \gamma_{yz}^0 \\ \gamma_{xz}^0 \end{Bmatrix}, \quad \varepsilon_{zz} = g'(z)\varepsilon_z^0 \qquad (9b)$$

where

$$\begin{Bmatrix} \varepsilon_x^0 \\ \varepsilon_y^0 \\ \gamma_{xy}^0 \end{Bmatrix} = \begin{Bmatrix} \dfrac{\partial u_0}{\partial x} \\ \dfrac{\partial v_0}{\partial x} \\ \dfrac{\partial u_0}{\partial y} + \dfrac{\partial v_0}{\partial x} \end{Bmatrix}, \quad \begin{Bmatrix} k_x^b \\ k_y^b \\ k_{xy}^b \end{Bmatrix} = \begin{Bmatrix} -\dfrac{\partial^2 w_0}{\partial x^2} \\ -\dfrac{\partial^2 w_0}{\partial y^2} \\ -2\dfrac{\partial^2 w_0}{\partial x \partial y} \end{Bmatrix}, \qquad (10a)$$

$$\begin{Bmatrix} k_x^s \\ k_y^s \\ k_{xy}^s \end{Bmatrix} = \begin{Bmatrix} k_1\theta \\ k_2\theta \\ k_1\dfrac{\partial}{\partial y}\int \theta\, dx + k_2\dfrac{\partial}{\partial x}\int \theta\, dy \end{Bmatrix} \qquad (10b)$$

$$\begin{Bmatrix} \gamma_{yz}^0 \\ \gamma_{xz}^0 \end{Bmatrix} = \begin{Bmatrix} k_2\int \theta\, dy + \dfrac{\partial \varphi_z}{\partial y} \\ k_1\int \theta\, dx + \dfrac{\partial \varphi_z}{\partial x} \end{Bmatrix}, \qquad \varepsilon_z^0 = \varphi_z \qquad (10c)$$

and

$$g'(z) = \frac{dg(z)}{dz} \qquad (11)$$

The integrals used in the above equations shall be resolved by a Navier type method and can be written as follows:

$$\frac{\partial}{\partial y}\int \theta\, dx = A'\frac{\partial^2 \theta}{\partial x \partial y}, \quad \frac{\partial}{\partial x}\int \theta\, dy = B'\frac{\partial^2 \theta}{\partial x \partial y},$$
$$\int \theta\, dx = A'\frac{\partial \theta}{\partial x}, \quad \int \theta\, dy = B'\frac{\partial \theta}{\partial y} \qquad (12)$$

where the coefficients A' and B' are expressed according to the type of solution employed, in this case by using Navier. Therefore, A' and B' are expressed as follows:

$$A' = -\frac{1}{\alpha^2}, \quad B' = -\frac{1}{\beta^2}, \quad k_1 = \alpha^2, \quad k_2 = \beta^2 \qquad (13)$$

where α and β are defined in expression (35).

The constitutive relations of a FG plate can be expressed as

$$\begin{Bmatrix} \sigma_x \\ \sigma_y \\ \sigma_z \\ \tau_{yz} \\ \tau_{xz} \\ \tau_{xy} \end{Bmatrix} = \begin{bmatrix} C_{11} & C_{12} & C_{13} & 0 & 0 & 0 \\ C_{12} & C_{22} & C_{23} & 0 & 0 & 0 \\ C_{13} & C_{23} & C_{33} & 0 & 0 & 0 \\ 0 & 0 & 0 & C_{44} & 0 & 0 \\ 0 & 0 & 0 & 0 & C_{55} & 0 \\ 0 & 0 & 0 & 0 & 0 & C_{66} \end{bmatrix} \begin{Bmatrix} \varepsilon_x \\ \varepsilon_y \\ \varepsilon_z \\ \gamma_{yz} \\ \gamma_{xz} \\ \gamma_{xy} \end{Bmatrix} \qquad (14)$$

where $(\sigma_x, \sigma_y, \sigma_z, \tau_{yz}, \tau_{xz}, \tau_{xy})$ and $(\varepsilon_x, \varepsilon_y, \varepsilon_z, \gamma_{yz}, \gamma_{xz}, \gamma_{xy})$ are stress and strain components, respectively.

The computation of the elastic constants C_{ij} depends on which assumption of ε_z are considered. If $\varepsilon_z = 0$, then C_{ij} are the plane stress-reduced elastic constants

$$C_{11} = C_{22} = \frac{E(z)}{1-v^2}, \quad C_{12} = v\, C_{11} \qquad (15a)$$

$$C_{44} = C_{55} = C_{66} = G(z) = \frac{E(z)}{2(1+v)}, \qquad (15b)$$

If $\varepsilon_z \neq 0$ (thickness stretching), then C_{ij} are 3D elastic constants, given by

$$C_{11} = C_{22} = C_{33} = \frac{(1-v)}{v}\lambda(z), \quad C_{12} = C_{13} = C_{23} = \lambda(z) \qquad (16a)$$

$$C_{44} = C_{55} = C_{66} = G(z) = \mu(z) = \frac{E(z)}{2(1+v)}, \qquad (16b)$$

Where $\lambda(z) = [vE(z)] / [(1-2v)(1+v)]$ and $\mu(z) = G(z) = E(z)/[2(1+v)] =$ Lame's coefficients.

The module E and G and the elastic coefficients C_{ij} vary through the thickness, according to Eqs. (3)-(5).

Next, Hamilton's energy principle is applied for deriving the equations of motion of the imperfect FG plates

$$0 = \int_0^T (\delta U_s + \delta U_F + \delta V - \delta K)\, dt \qquad (17)$$

Where δU_s is the virtual strain energy, δU_F additional strain energy induced by the elastic foundations and δV is the virtual work done by external applied forces and δK

The virtual strain energy is expressed by

$$\delta U_s = \iint_A \int_{-h/2}^{h/2} \begin{pmatrix} \sigma_x \delta\varepsilon_x + \sigma_y \delta\varepsilon_y + \sigma_z \delta\varepsilon_z + \sigma_{xy}\delta\gamma_{xy} + \\ \sigma_{xz}\delta\gamma_{xz} + \sigma_{yz}\delta\gamma_{yz} \end{pmatrix} dA\, dz$$

$$= \int_A \begin{bmatrix} N_x\dfrac{\partial \delta u_0}{\partial x} - M_x\dfrac{\partial^2 \delta w_0}{\partial x^2} + S_x k_1\theta + N_y\dfrac{\partial \delta v_0}{\partial y} - \\ M_y\dfrac{\partial^2 \delta w_0}{\partial y^2} + S_y k_2\theta + N_z\phi_z + N_{xy}\left(\dfrac{\partial \delta u_0}{\partial y} + \dfrac{\partial \delta v_0}{\partial x}\right) \\ -2M_{xy}\dfrac{\partial^2 \delta w_0}{\partial x \partial y} + S_{xy}\left(k_1 A'\dfrac{\partial^2 \delta\theta}{\partial x \partial y} + k_2 B'\dfrac{\partial^2 \delta\theta}{\partial x \partial y}\right) \\ + Q_{xz}\left(\dfrac{\partial \phi_z}{\partial x} + k_1 A'\dfrac{\partial \theta}{\partial x}\right) + Q_{yz}\left(\dfrac{\partial \phi_z}{\partial y} + k_2 B'\dfrac{\partial \theta}{\partial y}\right) \end{bmatrix} dx\, dy \qquad (18)$$

Where $N, M.S$ and Q are the stress resultants defined by

$$(N_i, M_i, S_i) = \int_{-h/2}^{h/2} (1, z, f)\sigma_i\, dz, \qquad i = x, y, xy \qquad (19a)$$

$$Q_i = \int_{-h/2}^{h/2} g(z)\sigma_i\, dz, \qquad i = xy, yz \qquad (19b)$$

$$N_z = \int_{-h/2}^{h/2} \sigma_z\, g'(z)\, dz \qquad (19c)$$

The strain energy induced by elastic foundations can be defined as

$$\delta U_F = \int_A \int_{-h/2}^{h/2} (U_{Winkler} + U_{Pasternak} + U_{Kerr})\, dA\, dz$$
$$= P_{Winkler} + P_{Pasternak} + P_{Kerr} \qquad (20)$$

In the case of Winkler foundation model, the distributed load can be defined by

$$P_{Winkler} = K_w(w_0 + g\varphi_z) \qquad (21)$$

where K_w is the modulus of subgrade reaction (elastic coefficient of the foundation).

The Pasternak model foundation is a two-parameter elastic model, which consists of a shear layer parameter with stiffness G_x, G_y are the shear moduli of the subgrade (shear layer foundation stiffness). If the foundation is homogeneous and isotropic, we will get $G_x=G_y=G$ and K_w is the modulus of subgrade reaction (springs stiffness). So, the distributed reaction between Pasternak foundation model and the lower surface of FG plate can be defined by

$$P_{Pasternak} = K_w \left(w_0 + g\phi_z \right)$$
$$-G_{px} \frac{\partial^2 \left(w_0 + g\phi_z \right)}{\partial x^2} - G_{py} \frac{\partial^2 \left(w_0 + g\phi_z \right)}{\partial y^2} \tag{22}$$

Clearly, the Pasternak model can reduce to the Winkler foundation model when considering $G_{px}=G_{py}=0$. The Kerr model foundation is a three-parameter elastic model consists of a shear layer (with stiffness K_s) independent upper (with stiffness K_u) and lower (with stiffness K_l) elastic layers (modeled by distributed springs). The distributed reaction of Kerr foundation model is defined as follow (Kneifati 1985)

$$P_{Kerr} = \left(\frac{K_l K_u}{K_l + K_u} \right) \left(w_0 + g\phi_z \right)$$
$$- \left(\frac{K_s K_u}{K_l + K_u} \right) \left[\frac{\partial^2 \left(w_0 + g\phi_z \right)}{\partial x^2} + \frac{\partial^2 \left(w_0 + g\phi_z \right)}{\partial y^2} \right] \tag{23}$$

Since the employed Kerr foundation has not been considered for the displacement field of quasi-3D plate theories, it is a novel work in the open literature.

The variation of the work done by the external applied forces can be expressed as

$$\delta V = -\int_A q \delta w dx dy = -\int_A \left(\delta w_0 + g(z) \delta \varphi \right)_z dx dy \tag{24}$$

The variation of kinetic energy is expressed as

$$\delta K = \int_\Omega \int_{-\frac{h}{2}}^{\frac{h}{2}} \rho(z) \left[\dot{u}\delta \dot{u} + \dot{v}\delta \dot{v} + \dot{w}\delta \dot{w} \right] dz d\Omega$$

$$= \int_\Omega \left\{ \begin{array}{l} I_0 \left[\dot{u}_0 \delta \dot{u}_0 + \dot{v}_0 \delta \dot{v}_0 + \dot{w}_0 \delta \dot{w}_0 \right] \\ -I_1 \left[\dot{u}_0 \frac{\partial \delta \dot{w}_0}{\partial x} + \frac{\partial \dot{w}_0}{\partial x} \delta \dot{u}_0 + \dot{v}_0 \frac{\partial \delta \dot{w}_0}{\partial y} + \frac{\partial \dot{w}_0}{\partial y} \delta \dot{v}_0 \right] \\ +I_2 \left[\frac{\partial \dot{w}_0}{\partial x} \frac{\partial \delta \dot{w}_0}{\partial x} + \frac{\partial \dot{w}_0}{\partial y} \frac{\partial \delta \dot{w}_0}{\partial y} \right] \\ -J_1 \left[\begin{array}{l} k_1 A' \dot{u}_0 \frac{\partial \delta \dot{\theta}}{\partial x} + k_1 A' \delta \dot{u}_0 \frac{\partial \dot{\theta}}{\partial x} \\ +k_2 \dot{v}_0 \frac{\partial \delta \dot{\theta}}{\partial y} + k_2 B' \delta \dot{v}_0 \frac{\partial \dot{\theta}}{\partial y} \end{array} \right] \\ +J_2 \left[\begin{array}{l} k_1 A' \frac{\partial \dot{w}_0}{\partial x} \frac{\partial \delta \dot{\theta}}{\partial x} + k_1 A' \frac{\partial \delta \dot{w}_0}{\partial x} \frac{\partial \dot{\theta}}{\partial x} + \\ k_2 B' \frac{\partial \dot{w}_0}{\partial y} \frac{\partial \delta \dot{\theta}}{\partial y} + k_2 B' \frac{\partial \delta \dot{w}_0}{\partial y} \frac{\partial \dot{\theta}}{\partial y} \end{array} \right] \\ +K_2 \left[k_1^2 A'^2 \frac{\partial \dot{\theta}}{\partial x} \frac{\partial \delta \dot{\theta}}{\partial x} + k_2^2 B'^2 \frac{\partial \dot{\theta}}{\partial y} \frac{\partial \delta \dot{\theta}}{\partial y} \right] + \\ J_1^s \left[\dot{w}_0 \delta \dot{\phi}_z + \dot{\phi}_z \delta \dot{w}_0 \right] + K_2^s \dot{\phi}_z \delta \dot{\phi}_z \end{array} \right\} d\Omega \tag{25}$$

where dot-superscript convention indicates the differentiation with respect to the time variable t; $\rho(z)$ is the mass density; and (I_0, I_1, J_1, J_1^s, I_2, J_2, K_2, K_2^s) are the mass inertias defined as

$$\left(I_0, I_1, J_1, J_1^s, I_2, J_2, J_3, J_3^s \right) =$$
$$\int_{-\frac{h}{2}}^{\frac{h}{2}} \left(1, z, f, g, z^2, zf, f^2, g^2 \right) \rho(z) dz \tag{26}$$

Substituting Eqs. (18), (20), (24) and (25) into Eq. (17) and integrating by parts, and collecting the coefficients of $\left(\delta u_0, \delta v_0, \delta w_0, \delta \theta, \delta \varphi_z \right)$, the following equations of motion are obtained

$$\delta u_0 : \frac{\partial N_x}{\partial x} + \frac{\partial N_{xy}}{\partial y} = I_0 \frac{\partial^2 u_0}{\partial t^2} - I_1 \frac{\partial^3 w_0}{\partial x \partial t^2} + J_1 \frac{\partial^3 \theta}{\partial x \partial t^2}$$

$$\delta v_0 : \frac{\partial N_{xy}}{\partial x} + \frac{\partial N_y}{\partial y} = I_0 \frac{\partial^2 v_0}{\partial t^2} - I_1 \frac{\partial^3 w_0}{\partial y \partial t^2} + J_1 \frac{\partial^3 \theta}{\partial y \partial t^2}$$

$$\delta w_0 : \frac{\partial^2 M_x}{\partial x^2} + \frac{\partial^2 M_y}{\partial y^2} + 2\frac{\partial^2 M_{xy}}{\partial x \partial y} + P_{Winkler} + P_{Pasternak}$$

$$+P_{Kerr} + q = I_0 \frac{\partial^2 w_0}{\partial t^2} + I_1 \left(\frac{\partial^3 u_0}{\partial x \partial t^2} + \frac{\partial^3 v_0}{\partial y \partial t^2} \right)$$

$$-I_2 \left(\frac{\partial^4 w_0}{\partial x^2 \partial t^2} + \frac{\partial^4 w_0}{\partial y^2 \partial t^2} \right) + J_2 \left(\frac{\partial^4 \theta}{\partial x^2 \partial t^2} + \frac{\partial^4 \theta}{\partial y^2 \partial t^2} \right) + J_1^s \frac{\partial^2 \phi_z}{\partial t^2}$$

$$\delta \theta : -k_1 S_x - k_2 S_y + 2\frac{\partial^2 S_{xy}}{\partial x \partial y} - \frac{\partial Q_{xz}}{\partial x} - \frac{\partial Q_{yz}}{\partial y} =$$

$$-J_1 \left(\frac{\partial^3 u_0}{\partial x \partial t^2} + \frac{\partial^3 v_0}{\partial y \partial t^2} \right) + J_2 \left(\frac{\partial^4 w_0}{\partial x^2 \partial t^2} + \frac{\partial^4 w_0}{\partial y^2 \partial t^2} \right)$$

$$-J_3 \left(\frac{\partial^4 \theta}{\partial x^2 \partial t^2} + \frac{\partial^4 \theta}{\partial y^2 \partial t^2} \right)$$

$$\delta \phi_z : \frac{\partial Q_{xz}}{\partial x} + \frac{\partial Q_{yz}}{\partial y} - N_z + P_{Winkler} + P_{Pasternak} + P_{Kerr} =$$

$$J_1^s \frac{\partial^2 w_0}{\partial t^2} + J_3^s \frac{\partial^2 \phi_z}{\partial t^2} \tag{27}$$

and the following boundary conditions are obtained at ($x=0,a$) and ($y=0,b$)

$$u_0 = v_0 = w_0 = \theta = \frac{\partial w_0}{\partial x} = 0, \quad at\ x = 0, a \tag{28a}$$

$$u_0 = v_0 = w_0 = \theta = \frac{\partial w_0}{\partial y} = 0, \quad at\ y = 0, b \tag{28b}$$

Substituting Eq. (9) into Eq. (14) the subsequent results into Eq. (19), the stress resultants are obtained as

$$\begin{Bmatrix} N_x \\ N_y \\ N_{xy} \\ M_x \\ M_y \\ M_{xy} \\ S_x \\ S_y \\ S_{xy} \\ N_z \end{Bmatrix} = \begin{bmatrix} A_{11} & A_{12} & 0 & B_{11} & B_{12} & 0 & B_{11}^s & B_{12}^s & 0 & L \\ A_{12} & A_{22} & 0 & B_{12} & B_{22} & 0 & B_{12}^s & B_{22}^s & 0 & L \\ 0 & 0 & A_{66} & 0 & 0 & B_{66} & 0 & 0 & B_{66}^s & 0 \\ B_{11} & B_{12} & 0 & D_{11} & D_{12} & 0 & D_{11}^s & D_{12}^s & 0 & L^a \\ B_{12} & B_{22} & 0 & D_{12} & D_{22} & 0 & D_{12}^s & D_{22}^s & 0 & L^a \\ 0 & 0 & B_{66} & 0 & 0 & D_{66} & 0 & 0 & D_{66}^s & 0 \\ B_{11}^s & B_{12}^s & 0 & D_{11}^s & D_{12}^s & 0 & H_{11}^s & H_{12}^s & 0 & R \\ B_{12}^s & B_{22}^s & 0 & D_{12}^s & D_{22}^s & 0 & H_{12}^s & H_{22}^s & 0 & R \\ 0 & 0 & B_{66}^s & 0 & 0 & D_{66}^s & 0 & 0 & H_{66}^s & 0 \\ L & L & 0 & L^a & L^a & 0 & R & R & 0 & Z \end{bmatrix} \begin{Bmatrix} \varepsilon_x^0 \\ \varepsilon_y^0 \\ \gamma_{xy}^0 \\ k_x^b \\ k_y^b \\ k_{xy}^b \\ k_x^s \\ k_y^s \\ k_{xy}^s \\ \varepsilon_z^0 \end{Bmatrix} \tag{29a}$$

$$\begin{Bmatrix} Q_{yz} \\ Q_{xz} \end{Bmatrix} = \begin{bmatrix} A_{44}^s & 0 \\ 0 & A_{55}^s \end{bmatrix} \begin{Bmatrix} \gamma_{yz}^0 \\ \gamma_{xz}^0 \end{Bmatrix} \tag{29b}$$

where

$$\begin{Bmatrix} A_{11} & B_{11} & D_{11} & B_{11}^s & D_{11}^s & H_{11}^s \\ A_{12} & B_{12} & D_{12} & B_{12}^s & D_{12}^s & H_{12}^s \\ A_{66} & B_{66} & D_{66} & B_{66}^s & D_{66}^s & H_{66}^s \end{Bmatrix} = \tag{30a}$$

$$\int_{-\frac{h}{2}}^{\frac{h}{2}} \lambda(z) \left[1, z, z^2, f, z f, f^2 \right] \begin{Bmatrix} \dfrac{1-\nu}{\nu} \\ 1 \\ \dfrac{1-2\nu}{2\nu} \end{Bmatrix} dz$$

$$\begin{Bmatrix} L \\ L^a \\ R \\ Z \end{Bmatrix} = \int_{-\frac{h}{2}}^{\frac{h}{2}} \lambda(z) \begin{Bmatrix} 1 \\ z \\ f \\ g' \dfrac{1-\nu}{\nu} \end{Bmatrix} g' dz \tag{30b}$$

Where

$$\lambda(z) = \frac{E(z)\nu(z)}{[1+\nu(z)][1-2\nu(z)]} \text{ and } \mu(z) = \frac{E(z)}{2[1+\nu(z)]} \tag{30c}$$

By substituting Eq. (29) into Eq. (27), the equations of motion can be expressed in terms of displacements $(\delta u_0, \delta v_0, \delta w_0, \delta\vartheta, \delta\varphi_z)$ as

$$\delta u_0 : L_1 u_0 + A_{11} L_2 v_0 - L_3 \frac{\partial w_0}{\partial x} + L_4 \frac{\partial \theta}{\partial x} + L \frac{\partial \varphi_z}{\partial x} = 0$$

$$\delta v_0 : A_{11} L_2 u_0 + L_5 v_0 - L_3 \frac{\partial w_0}{\partial y} + L_6 \frac{\partial \theta}{\partial y} + L \frac{\partial \varphi_z}{\partial y} = 0$$

$$\delta w_0 : L_3 \left(\frac{\partial u_0}{\partial x} + \frac{\partial v_0}{\partial y} \right) - L_7 w_0 + L_8 \theta + L_9 \varphi_z = 0 \tag{31}$$

$$\delta\vartheta : -L_4 \frac{\partial u_0}{\partial x} - L_6 \frac{\partial v_0}{\partial y} + L_8 w_0 - L_{10}\theta + L_{11}\varphi_z = 0$$

$$\delta\varphi_z : L \left(\frac{\partial u_0}{\partial x} + \frac{\partial v_0}{\partial y} \right) + L_9 w_0 + L_{13}\theta + L_{14}\varphi_z = 0$$

where the operator L_i are given by

$$L_1 = A_{11}\nabla_x^2 - I_0 \frac{\partial^2}{\partial t^2} , L_2 = (\nu + \bar{\nu})\frac{\partial^2}{\partial x \partial y}, L_3 = B_{11}\nabla^2 - I_1 \frac{\partial^2}{\partial t^2}$$

$$L_4 = B_{11}^s \left((k_1 + k_2\nu) + \bar{\nu}(k_1 A' + k_2 B')\frac{\partial^2}{\partial y^2} \right) - J_1 k_1 A' \frac{\partial^2}{\partial t^2},$$

$$L_5 = A_{11}\nabla_y^2 - I_0 \frac{\partial^2}{\partial t^2}$$

$$L_6 = B_{11}^s \left((k_1\nu + k_2) + \bar{\nu}(k_1 A' + k_2 B')\frac{\partial^2}{\partial x^2} \right) - J_1 k_2 B' \frac{\partial^2}{\partial t^2},$$

$$L_7 = D_{11}\nabla^4 + (I_0 - I_2\nabla^2)\frac{\partial^2}{\partial t^2} + K_w - G_p\nabla^2 + \left(\frac{K_l K_u}{K_l + K_u} \right)$$
$$- \left(\frac{K_s K_u}{K_l + K_u} \right)\nabla^2 \tag{32}$$

$$L_8 = D_{11}^s \begin{pmatrix} (k_1 + k_2\nu)\dfrac{\partial^2}{\partial x^2} + 2(k_1 A' + k_2 B')\bar{\nu}\dfrac{\partial^4}{\partial x^2 \partial y^2} \\ + (k_1\nu + k_2)\dfrac{\partial^2}{\partial y^2} \end{pmatrix}$$
$$- J_2 \left(k_1 A' \frac{\partial^2}{\partial x^2} + k_2 B' \frac{\partial^2}{\partial y^2} \right)\frac{\partial^2}{\partial t^2}$$

$$L_8 = D_{11}^s \begin{pmatrix} (k_1 + k_2\nu)\dfrac{\partial^2}{\partial x^2} + 2(k_1 A' + k_2 B')\bar{\nu}\dfrac{\partial^4}{\partial x^2 \partial y^2} \\ + (k_1\nu + k_2)\dfrac{\partial^2}{\partial y^2} \end{pmatrix}$$

$$L_9 = L^a\nabla^2 - J_1^s \frac{\partial^2}{\partial t^2} + g \begin{pmatrix} K_w - G\nabla^2 + \left(\dfrac{K_l K_u}{K_l + K_u} \right) \\ - \left(\dfrac{K_s K_u}{K_l + K_u} \right)\nabla^2 \end{pmatrix}$$

$$L_{10} = H_{11}^s \left(k_1^2 + 2\nu k_1 k_2 + k_2^2 \right)$$
$$+ \left(\left(\bar{\nu}H_{11}^s (k_1 A' + k_2 B')\frac{\partial^2}{\partial y^2} - (k_1 A')^2 A^s \right) - (k_1 A')^2 K_2 \frac{\partial^2}{\partial t^2} \right)\frac{\partial^2}{\partial x^2}$$
$$+ \left(\left(\bar{\nu}H_{11}^s (k_1 A' + k_2 B')\frac{\partial^2}{\partial x^2} - (k_2 B')^2 A^s \right) - (k_2 B')^2 K_2 \frac{\partial^2}{\partial t^2} \right)\frac{\partial^2}{\partial y^2}$$

$$L_{11} = A^s \left(k_1 A' \frac{\partial^2}{\partial x^2} + k_2 B' \frac{\partial^2}{\partial y^2} \right) - R(k_1 + k_2)$$

$$L_{12} = A^s\nabla^2 - R^a - K_2^s \frac{\partial^2}{\partial t^2} + g \begin{pmatrix} K_w - G_p\nabla^2 + \left(\dfrac{K_l K_u}{K_l + K_u} \right) \\ - \left(\dfrac{K_s K_u}{K_l + K_u} \right)\nabla^2 \end{pmatrix}$$

$$L_{13} = A^s \left(k_1 A' \frac{\partial^2}{\partial x^2} + k_2 B' \frac{\partial^2}{\partial y^2} \right),$$

$$L_{14} = A^s\nabla^2 + Z - K_2^s \frac{\partial^2}{\partial t^2} + g \begin{pmatrix} K_w - G_p\nabla^2 + \left(\dfrac{K_l K_u}{K_l + K_u} \right) \\ - \left(\dfrac{K_s K_u}{K_l + K_u} \right)\nabla^2 \end{pmatrix}$$

in which

$$\nabla_x^2 = \frac{\partial^2}{\partial x^2} + \bar{\nu}\frac{\partial^2}{\partial y^2}, \qquad \nabla_y^2 = \frac{\partial^2}{\partial y^2} + \bar{\nu}\frac{\partial^2}{\partial x^2},$$
$$\nabla^2 = \frac{\partial^2}{\partial x^2} + \frac{\partial^2}{\partial y^2}, \qquad \nabla^4 = \nabla^2(\nabla^2), \qquad \bar{\nu} = \frac{1-\nu}{2} \tag{33}$$

3.2 Analytical solutions

In this section, analytical solutions for bending and free vibration are presented for a simply supported rectangular plate under transverse load q. Based on the Navier approach, the solutions are assumed as

$$\begin{Bmatrix} u_0(x,y,t) \\ v_0(x,y,t) \\ w_0(x,y,t) \\ \theta(x,y,t) \end{Bmatrix} = \sum_{m=1}^{\infty} \sum_{n=1}^{\infty} \begin{Bmatrix} U_{mn}\cos(\alpha x)\sin(\beta y)e^{i\omega t} \\ V_{mn}\sin(\alpha x)\cos(\beta y)e^{i\omega t} \\ W_{mn}\sin(\alpha x)\sin(\beta y)e^{i\omega t} \\ \Theta_{mn}\sin(\alpha x)\sin(\beta y)e^{i\omega t} \end{Bmatrix} \tag{34}$$

where U_{mn}, V_{mn}, W_{mn}, Θ_{mn}, are Fourier coefficients to be

determined for each pair of m and n.

with

$$\alpha = m\pi/a, \quad \beta = n\pi/b \quad (35)$$

The transverse load q is expanded in the double-Fourier sine series as

$$q(x,y) = \sum_{m=1}^{\infty}\sum_{n=1}^{\infty} Q_{mn}\sin\alpha x\sin\beta y \quad (36)$$

Where

$$Q_{mn} = \frac{4}{ab}\int_0^a\int_0^b q(x,y)\sin\alpha x\sin\beta y\,dxdy$$

$$= \begin{cases} q_0 & \text{for sinusoidally distributed load,} \\ \dfrac{16q_0}{mn\pi^2} & \text{for uniformaly distributed load} \end{cases} \quad (37)$$

Substituting Eqs. (34) and (36) into Eq. (31), the analytical solutions can be obtained from the following equations

$$\left\{ \begin{bmatrix} s_{11} & s_{12} & s_{13} & s_{14} & s_{15} \\ s_{12} & s_{22} & s_{23} & s_{24} & s_{25} \\ s_{13} & s_{23} & s_{33} & s_{34} & s_{35} \\ s_{14} & s_{24} & s_{34} & s_{44} & s_{45} \\ s_{15} & s_{25} & s_{35} & s_{45} & s_{55} \end{bmatrix} - \omega^2 \begin{bmatrix} m_{11} & 0 & m_{13} & m_{14} & 0 \\ 0 & m_{22} & m_{23} & m_{24} & 0 \\ m_{13} & m_{23} & m_{33} & m_{34} & m_{35} \\ m_{14} & m_{24} & m_{34} & m_{44} & 0 \\ 0 & 0 & m_{35} & 0 & m_{55} \end{bmatrix} \right\} \begin{Bmatrix} U_{mn} \\ V_{mn} \\ W_{mn} \\ \Theta_{mn} \\ \varphi_{mn} \end{Bmatrix} = \begin{Bmatrix} 0 \\ 0 \\ Q_{mn} \\ 0 \\ 0 \end{Bmatrix} \quad (38)$$

Where

$$s_{11} = A_{11}(\alpha^2 + \bar{v}\beta^2)$$
$$s_{12} = \alpha\beta A_{11}(v + \bar{v})$$
$$s_{13} = -B_{11}[(v + 2\bar{v})\alpha\beta^2 + \alpha^3]$$
$$s_{14} = B_{11}^s\alpha[(k_1 + vk_2) - \bar{v}(k_1A' + k_2B')\beta^2]$$
$$s_{15} = -L\alpha$$
$$s_{22} = A_{11}(\beta^2 + \bar{v}\alpha^2)$$
$$s_{23} = B_{11}\beta(\alpha^2 + \beta^2)$$
$$s_{24} = B_{11}^s\beta[(vk_1 + k_2) - \bar{v}(k_1A' + k_2B')\alpha^2]$$
$$s_{25} = -L\beta \quad (39)$$
$$s_{33} = D_{11}(\alpha^2 + \beta^2)^2 + P_{foundation}$$
$$s_{34} = D_{11}^s[-k_1(\alpha^2 + v\beta^2) + 2\bar{v}(k_1A' + k_2B')\alpha^2\beta^2 - k_2(v\alpha^2 + \beta^2)]$$
$$s_{35} = L^a(\alpha^2 + \beta^2) + gP_{foundation}$$
$$s_{44} = H_{11}^s\left(k_1^2 + k_2^2 + 2vk_1k_2 + \bar{v}(k_1A' + k_2B')^2\alpha^2\beta^2\right) + A^s\left(k_1^2A'^2\alpha^2 + k_2^2B'^2\beta^2\right)$$
$$s_{45} = -A^s\left(k_1A'\alpha^2 + k_2B'\beta^2\right) - R(k_1 + k_2)$$
$$s_{55} = A^s(\alpha^2 + \beta^2) + Z + gP_{foundation}$$

Table 1 Material properties of FGM constituents

Material	Material Properties		
	Elasticity Modulus, E [GPa]	Density, ρ [kg/m^3]	Poisson's Ratio, v
Aluminum (Al)	$E_m = 70$	$\rho_m = 2702$	$v = 0.3$
Alumina (Al$_2$O$_3$)	$E_c = 380$	$\rho_c = 3800$	$v = 0.3$

where m_{ij} are the elements of generalized mass matrix and the specific expressions of them are also given by

$$m_{11} = I_0,$$
$$m_{13} = -\alpha I_1,$$
$$m_{14} = -J_1k_1A'\alpha,$$
$$m_{22} = I_0,$$
$$m_{23} = -\beta I_1, \quad m_{24} = -J_1k_2B'\beta,$$
$$m_{33} = I_0 + I_2(\alpha^2 + \beta^2),$$
$$m_{34} = J_2(k_1A'\alpha^2 + k_2B'\beta^2),$$
$$m_{35} = J_1^s$$
$$m_{44} = J_3(k_1^2A'^2\alpha^2 + k_2^2B'^2\beta^2),$$
$$m_{55} = J_3^s$$

$$(40)$$

4. Numerical results and discussions

In this section, Numerical results for are presented and discussed to verify the accuracy of the present theory in predicting the bending and free vibration responses of simply supported of porous FG plates resting on elastic foundations chosen as Winkler, Pasternak or Kerr foundation. The present results are computed using the present quasi-3D theory with only 5 unknows. To illustrate the proposed approach, a ceramic-metal functionally graded plate is considered. Material properties of the used materials are shown in Table 1.

For convenience, the following dimensionless forms are used:

$$\bar{z} = \frac{z}{h}, \quad S = a/h, \quad \hat{w} = \frac{100E}{q_0hS^4}w\left(\frac{a}{2},\frac{b}{2},0\right),$$

$$\hat{\sigma}_x = \frac{1}{q_0S^2}\sigma_x\left(\frac{a}{2},\frac{b}{2},\frac{h}{2}\right), \quad \hat{\sigma}_y = \frac{1}{q_0S^2}\sigma_y\left(\frac{a}{2},\frac{b}{2},\frac{h}{2}\right)$$

$$\hat{\tau}_{xy} = \frac{1}{q_0S}\tau_{xy}\left(0,0,\frac{h}{2}\right), \quad \hat{\tau}_{xz} = \frac{1}{q_0S}\tau_{xz}\left(0,\frac{b}{2},0\right),$$

$$\hat{\tau}_{yz} = \frac{1}{q_0S}\tau_{yz}\left(\frac{a}{2},0,0\right), \quad \tilde{u} = \frac{100D_c}{q_0a^4}u\left(0,\frac{b}{2},-\frac{h}{2}\right),$$

$$\tilde{w} = \frac{100D_c}{q_0a^4}w\left(\frac{a}{2},\frac{b}{2},0\right), \quad \tilde{\sigma}_x = \frac{h^2}{q_0S^2}\sigma_x\left(\frac{a}{2},\frac{b}{2},-\frac{h}{2}\right),$$

$$\tilde{\tau}_{xy} = \frac{h^2}{q_0a^2}\tau_{xy}\left(0,0,-\frac{h}{2}\right), \quad \tilde{\tau}_{xz} = \frac{1}{q_0}\tau_{xz}\left(0,\frac{b}{2},0\right),$$

$$\bar{u} = \frac{100E_c}{q_0aS^3}u\left(\frac{a}{2},\frac{b}{2},\bar{z}\right), \quad \bar{w} = \frac{10E_c}{q_0aS^3}w\left(\frac{a}{2},\frac{b}{2},\bar{z}\right),$$

Table 2 Effect of normal strain ε_z on the dimensionless stresses and transversal displacement for isotropic square plate (*a/h*=10) subjected to a UD

Theory	$\hat{w}(a/2,b/2,0)$	$\hat{\sigma}_x(h/2)$	$\hat{\sigma}_y(h/2)$	$\hat{\tau}_{xy}(h/2)$	$\hat{\tau}_{xz}(0,b/2,0)$	$\hat{\tau}_{yz}(a/2,0,0)$
Exact 3D (Srinivas *et al.* 1970a)	4.639	0.290	0.290	/	0.488	/
Shimpi *et al.* (2003) $\varepsilon_z \neq 0$	4.625	0.307	0.307	0.195	0.505	0.505
Hebali *et al.* (2014) $\varepsilon_z \neq 0$	4.631	0.276	0.276	0.197	0.481	0.481
Benahmed *et al.* (2017) $\varepsilon_z \neq 0$	4.633	0.302	0.302	0.197	0.481	0.502
Present $\varepsilon_z \neq 0$	4.639	0.288	0.288	0.197	0.491	0.491

Table 3 Dimensionless in-plane longitudinal stress $\bar{\sigma}_x$ and displacement $\bar{w}$ for FG square plate subjected to a sinusoidal load

p	Theory	$\bar{\sigma}_x(h/3)$			$\bar{w}$ (*a/2, b/2, 0*)		
		a/h=4	*a/h*=10	*a/h*=100	*a/h*=4	*a/h*=10	*a/h*=100
1	Carrera *et al.* (2011) $\varepsilon_z \neq 0$	0.6221	1.5064	14.969	0.7171	0.5875	0.5625
	Neves *et al.* (2012) $\varepsilon_z \neq 0$	0.5925	1.4945	14.969	0.6997	0.5845	0.5624
	Hebali *et al.* (2014) $\varepsilon_z \neq 0$	0.5952	1.4954	14.963	0.6910	0.5686	0.5452
	Present $\varepsilon_z \neq 0$	0.5848	1.4623	14.619	0.6916	0.5695	0.5461
4	Carrera *et al.* (2011) $\varepsilon_z \neq 0$	0.4877	1.1971	11.923	1.1585	0.8821	0.8286
	Neves *et al.* (2012) $\varepsilon_z \neq 0$	0.4404	1.1783	11.932	1.1178	0.8750	0.8286
	Hebali *et al.* (2014) $\varepsilon_z \neq 0$	0.4507	1.1779	11.871	1.0964	0.8413	0.7926
	Present $\varepsilon_z \neq 0$	0.4375	1.1396	11.478	1.0983	0.8424	0.7934
10	Carrera *et al.* (2011) $\varepsilon_z \neq 0$	0.1478	0.8965	8.9077	1.3745	1.0072	0.9361
	Neves *et al.* (2012) $\varepsilon_z \neq 0$	0.3227	1.1783	11.932	1.3490	0.8750	0.8286
	Hebali *et al.* (2014) $\varepsilon_z \neq 0$	0.3325	0.8889	8.9977	1.3333	0.9791	0.9114
	Present $\varepsilon_z \neq 0$	0.3136	0.8549	8.6648	1.3506	0.9791	0.9143

$$\bar{\sigma}_x = \frac{1}{q_0 S}\sigma_x\left(\frac{a}{2},\frac{b}{2},\bar{z}\right), \quad \bar{\tau}_{xy} = \frac{1}{q_0 S}\tau_{xy}\left(0,0,\bar{z}\right),$$

$$\bar{\tau}_{xz} = \frac{1}{q_0 S}\tau_{xz}\left(0,\frac{b}{2},\bar{z}\right), \quad k_w^* = \frac{K_w a^4}{h^3}, \quad k_s^* = \frac{K_s a^2}{h^3 v} = \frac{K_s b^2}{h^3 v},$$

$$\bar{K}_w = \frac{K_w a^4}{D_m}, \quad \bar{G}_p = \frac{G_p a^2}{D_m}, \quad \bar{K}_l = \frac{K_l a^4}{D_m}, \quad \bar{K}_u = \frac{K_u a^4}{D_m}, \quad \bar{K}_s = \frac{K_s a^2}{D_m},$$

$$D_m = \left(E_m h^3\right)\big/\left(12\left(1-v_m^2\right)\right), \quad \hat{\omega} = \omega h\sqrt{\rho/G}, \quad \tilde{\omega} = \omega h\sqrt{\rho_m/E_m},$$

$$\bar{\omega} = \omega \frac{a^2}{h}\sqrt{\rho_m/E_m}$$

4.1 Results of bending analysis

In order to verify the numerical precision of the theory and the formulation, we obtained the results of stresses and transversal displacement for homogeneous isotropic plates (*p*=0) subjected to uniform load by the current theory and compared to those obtained for bending by the exact solution carried out by Srinivas *et al.* (1970) and quasi-3D solutions given by Shimpi *et al.* (2003), Hebali *et al.* (2014) and Benahmed *et al.* (2017) as shown in Table 2. The agreeability between the present results and the published ones can be clearly noted.

Table 3 shows the non-dimensional transverse displacement $\bar{w}$ and axial stress $\bar{\sigma}_x$ for thick square plates subjected to a sinusoidal load. The obtained results are compared with quasi-3D solutions given by Neves *et al.* (2012), Hebali *et al.* (2014) and with those obtained using finite element approximations by Carrera *et al.* (2011). It can be observed that our results are in an excellent

agreement to those predicted using theories that consider thickness stretching.

Table 4 exhibit the effects of foundation stiffness and power index *p* on non-dimensional displacement and stress components of simply supported rectangular plate under uniformly distributed load and as compared with those given by Thai and Choi (2011) and Zenkour and Sobhy (2013) in which the thickness stretching effect is neglected ($\varepsilon_z = 0$), we see that the results overestimates the deflections and stresses, and this is attributable to the thickness stretching effect, which is omitted in the theories developed by these references. Also, it can be observed from the table that the results of quasi-3D shear deformation theories given by Benahmed *et al.* (2017) are in an excellent agreement for all values of the power-law index and foundation stiffness.

Afterhaving proceeded to the validation of the current quasi-3D theory of the plates. We wish to study the influence of the effect of normal deformation (stretching effect) on the performance of imperfect plates containing porosities. Table 5 shows the effect of power index *p* on the non-dimensional displacement and stress components of square plates subjected to sinusoidal loading (*a/h*=10) and non-porous functional levels (*α*=0) and compared to those given by Zenkour (2006), Thai and Kim (2013), Mantari. *et al.* (2012) and Nguyen *et al.* (2014) without stretching effect ($\varepsilon_z = 0$) and quasi-3D solutions with stretching effect ($\varepsilon_z \neq 0$) given by Carrera *et al*, 2008 and Wu and Chiu, 2011. Table 5 shows that excellent agreement is obtained for all values of the power law index. Then, the results of the non-dimensional displacement and stress components of

Table 4 Comparison of the displacements and stresses of simply supported rectangular plate under uniformly distributed load ($a=10h$, $b=3a$)

p	k_w^*	k_s^*	Theory	$\tilde{u}(-h/2)$	$\tilde{w}(0)$	$\tilde{\sigma}_x(-h/2)$	$\tilde{\tau}_{xy}(-h/2)$	$\tilde{\tau}_{xy}(0)$
0.5	0	0	Thai and Choi (2011)	0.3491	1.9345	0.2337	0.0941	-
			Zenkour and Sobhy (2013)	0.34919	1.93441	0.23372	0.09415	7.68354
			Benahmed *et al.* (2017)	0.33498	1.90215	0.23941	0.09007	7.56253
			Present $\varepsilon_{zz}\neq0$	0.33516	1.90422	0.23272	0.09026	7.38728
	100	0	Thai and Choi (2011)	0.3358	1.8590	0.2242	0.0916	-
			Zenkour and Sobhy (2013)	0.33586	1.85907	0.22424	0.09167	7.42978
			Benahmed *et al.* (2017)	0.32246	1.82955	0.22989	0.08774	7.31675
			Present $\varepsilon_{zz}\neq0$	0.32261	1.83143	0.22346	0.08793	7.14708
	100	100	Thai and Choi (2011)	0.3012	1.6640	0.1999	0.0850	-
			Zenkour and Sobhy (2013)	0.30131	1.66399	0.19989	0.08503	6.76069
			Benahmed *et al.* (2017)	0.28991	1.64138	0.20536	0.08151	6.66745
			Present $\varepsilon_{zz}\neq0$	0.29000	1.64282	0.19961	0.08168	6.51483
2	0	0	Thai and Choi (2011)	0.6564	3.2266	0.4395	0.1766	-
			Zenkour and Sobhy (2013)	0.65655	3.22672	0.43961	0.17666	6.91072
			Benahmed *et al.* (2017)	0.60340	3.07560	0.44695	0.16202	6.79513
			Present $\varepsilon_{zz}\neq0$	0.60465	3.08188	0.43926	0.16248	6.60914
	100	0	Thai and Choi (2011)	0.6156	3.0218	0.4105	0.1690	-
			Zenkour and Sobhy (2013)	0.61576	3.02190	0.41060	0.16906	6.53895
			Benahmed *et al.* (2017)	0.56771	2.88981	0.41881	0.15538	6.44548
			Present $\varepsilon_{zz}\neq0$	0.56881	2.89532	0.41156	0.15582	6.26874
	100	100	Thai and Choi (2011)	0.5186	2.5364	0.3423	0.1501	-
			Zenkour and Sobhy (2013)	0.51872	2.53642	0.34233	0.15020	5.63882
			Benahmed *et al.* (2017)	0.48189	2.44460	0.35187	0.13875	5.59033
			Present $\varepsilon_{zz}\neq0$	0.48267	2.44849	0.34570	0.13911	5.43906
5	0	0	Thai and Choi (2011)	0.7802	3.8506	0.5223	0.2103	-
			Zenkour and Sobhy (2013)	0.78046	3.85174	0.52237	0.21044	6.14557
			Benahmed *et al.* (2017)	0.72061	3.69376	0.53104	0.19389	6.03129
			Present $\varepsilon_{zz}\neq0$	0.72112	3.69681	0.52200	0.19418	5.82417
	100	0	Thai and Choi (2011)	0.7230	3.5620	0.4816	0.1996	-
			Zenkour and Sobhy (2013)	0.72323	3.56296	0.48167	0.19975	5.75485
			Benahmed *et al.* (2017)	0.66999	3.42857	0.49132	0.18445	5.66241
			Present $\varepsilon_{zz}\neq0$	0.67041	3.43116	0.48295	0.18472	5.46811
	100	100	Thai and Choi (2011)	0.5922	2.9046	0.3897	0.1740	-
			Zenkour and Sobhy (2013)	0.59231	2.90518	0.38971	0.17410	4.84302
			Benahmed *et al.* (2017)	0.55294	2.81786	0.40060	0.16159	4.79288
			Present $\varepsilon_{zz}\neq0$	0.55318	2.81942	0.39373	0.16182	4.63122

perfect and imperfect FG plates with a symmetric distribution (FGM I) are calculated and tabulated in Table 5. The comparisons between the current results and the available results obtained by Zenkour (2019) are in good agreement for all cases.

Table 6 exhibit the effects of the elastic foundation parameters ($\bar{K}_w$, $\bar{G}_p$) and side-tothickness ratio a/h on the deflections $\bar{w}$. For this, three types of pore distribution were considered, uniform distribution of porosities (FGM I), unequal distribution of porosities (FGM II) and imperfect materials with logarithm unequal distribution of porosities (FGM III). It is clear that for uneven porosity distributions the deflections $\bar{w}$ increase with the increase of the porosity volume fraction α without or resting on elastic foundation and deflections $\bar{w}$ decrease when a/h increase. In addition, the deflections are decreasing with the existence of the elastic foundations. The inclusion of the

Pasternak's foundation parameters gives results more than those with the inclusion of Winkler's foundation parameter

Table 7 exhibit the effects of the Kerr foundation parameters ($\bar{K}_u$, $\bar{K}_s$), volume fraction indices p and side-to-thickness ratio a/h on the non-dimensional deflection $\bar{w}$, of square isotropic and FG plates resting on Kerr foundation ($\bar{K}_l = 100$) on the basis of the present quasi-3D shear deformation plate theories. As it can be seen, that upper spring and shear layer parameter have rising effects. The shear parameter has more effect than the lower and upper spring constants. As another verification attempt, it can seen that the non-dimensional deflection $\bar{w}$ of FG plate embedded in Kerr foundation are small than those embedded in Winkler and Pasternak foundations due to an extra upper spring.

The variations of Non-dimensional stress $\bar{\sigma}_x$ of nonporous and porous FG square plates versus the Kerr

Table 5 Comparisons of dimensionless stresses and displacements of functionally graded porous square plates subjected to sinusoidal load

p	Methods		$a/h=10$				
			$\bar{u}(-h/4)$	$\bar{w}(0)$	$\bar{\sigma}_x(h/3)$	$\bar{\tau}_{xz}(h/6)$	$\bar{\tau}_{xy}(-h/3)$
0	Zenkour (2019) $\varepsilon_{zz}\neq 0$	$\alpha=0.0$	0.216337	0.293938	1.303085	0.212331	0.700122
		$\alpha=0.1$	0.229953	0.312438	1.303085	0.212331	0.700121
	Present	$\alpha=0.0$	0.216724	0.294236	1.322308	0.211924	0.701028
		$\alpha=0.1$	0.230364	0.312754	1.322308	0.211924	0.701028
1	Nguyen *et al.* (2014) $\varepsilon_{zz}=0$		0.641300	0.589000	1.489000	0.261100	0.611100
	Carrera *et al.* (2008) $\varepsilon_{zz}\neq 0$		0.643600	0.587500	1.506200	0.251000	0.608100
	Wu and Chiu (2011) $\varepsilon_{zz}\neq 0$		0.643600	0.587600	1.506100	0.251100	0.611200
	Zenkour (2006) $\varepsilon_{zz}=0$		0.662600	0.588900	1.489400	0.262200	0.611000
	Mantari *et al.* (2012) $\varepsilon_{zz}=0$		0.639800	0.588000	1.488800	0.256600	0.610900
	Thai and Kim (2013) $\varepsilon_{zz}=0$		0.641400	0.589000	1.489800	0.260800	0.611100
	Zenkour (2019) $\varepsilon_{zz}\neq 0$	$\alpha=0.0$	0.587959	0.569038	1.434203	0.261088	0.565518
		$\alpha=0.1$	0.701623	0.655782	1.458887	0.266506	0.546517
	Present	$\alpha=0.0$	0.588612	0.569540	1.462255	0.260588	0.566008
		$\alpha=0.1$	0.702349	0.656340	1.487920	0.265995	0.546960
2	Nguyen *et al.* (2014)		0.898200	0.757300	1.395900	0.274200	0.544200
	Carrera *et al.* (2008) $\varepsilon_{zz}\neq 0$		0.901200	0.757000	1.414700	0.249600	0.542100
	Wu and Chiu (2011) $\varepsilon_{zz}\neq 0$		0.901300	0.757100	1.413300	0.249500	0.543600
	Zenkour (2006) $\varepsilon_{zz}=0$		0.928100	0.757300	1.395400	0.276300	0.544100
	Mantari *et al.* (2012) $\varepsilon_{zz}=0$		0.895700	0.756400	1.394000	0.274100	0.543800
	Thai and Kim (2013) $\varepsilon_{zz}=0$		0.898400	0.757300	1.396000	0.273700	0.544200
	Zenkour (2019) $\varepsilon_{zz}\neq 0$	$\alpha=0.0$	0.807013	0.721361	1.325404	0.274742	0.493683
		$\alpha=0.1$	1.049624	0.885498	1.332625	0.284519	0.453813
	Present	$\alpha=0.0$	0.808897	0.722455	1.358142	0.273311	0.494670
		$\alpha=0.1$	1.052371	0.887131	1.366945	0.282911	0.454865
4	Nguyen *et al.* (2014)		1.050000	0.881600	1.179200	0.254600	0.566900
	Carrera *et al.* (2008) $\varepsilon_{zz}\neq 0$		1.054100	0.882300	1.198500	0.236200	0.566600
	Wu and Chiu (2011) $\varepsilon_{zz}\neq 0$		1.054100	0.882300	1.184100	0.236200	0.567100
	Zenkour (2006) $\varepsilon_{zz}=0$		1.094100	0.881900	1.178300	0.258000	0.566700
	Mantari *et al.* (2012) $\varepsilon_{zz}=0$		1.045700	0.881400	1.175500	0.262300	0.566200
	Thai and Kim (2013) $\varepsilon_{zz}=0$		1.050200	0.881500	1.179400	0.253700	0.566900
	Zenkour (2019) $\varepsilon_{zz}\neq 0$	$\alpha=0.0$	0.942715	0.841682	1.103477	0.255831	0.514100
		$\alpha=0.1$	1.310574	1.082177	1.043439	0.267216	0.479271
	Present	$\alpha=0.0$	0.944523	0.842353	1.139552	0.253065	0.514878
		$\alpha=0.1$	1.313739	1.083384	1.081856	0.263691	0.480244
8	Nguyen *et al.* (2014)		1.075900	0.974600	0.947300	0.209400	0.585700
	Carrera *et al.* (2008) $\varepsilon_{zz}\neq 0$		1.083000	0.973800	0.968700	0.226200	0.587900
	Wu and Chiu (2011) $\varepsilon_{zz}\neq 0$		1.083000	0.973900	0.962200	0.226100	0.588300
	Zenkour (2006) $\varepsilon_{zz}=0$		1.134000	0.975000	0.946600	0.212100	0.585600
	Mantari *et al.* (2012) $\varepsilon_{zz}=0$		1.070900	0.973700	0.943100	0.214000	0.585000
	Thai and Kim (2013) $\varepsilon_{zz}=0$		1.076300	0.974600	0.947700	0.208800	0.585800
	Zenkour (2019) $\varepsilon_{zz}\neq 0$	$\alpha=0.0$	0.982899	0.944138	0.886117	0.210366	0.540509
		$\alpha=0.1$	1.393026	1.232257	0.785381	0.210846	0.511665
	Present	$\alpha=0.0$	0.982757	0.943841	0.920533	0.208281	0.540263
		$\alpha=0.1$	1.393060	1.231426	0.822481	0.208014	0.511488

Table 6 Variations of deflection $\bar{w}(0)$ of perfect and imperfect FG square plates versus the Winkler-Pasternak foundation stiffness (p=1)
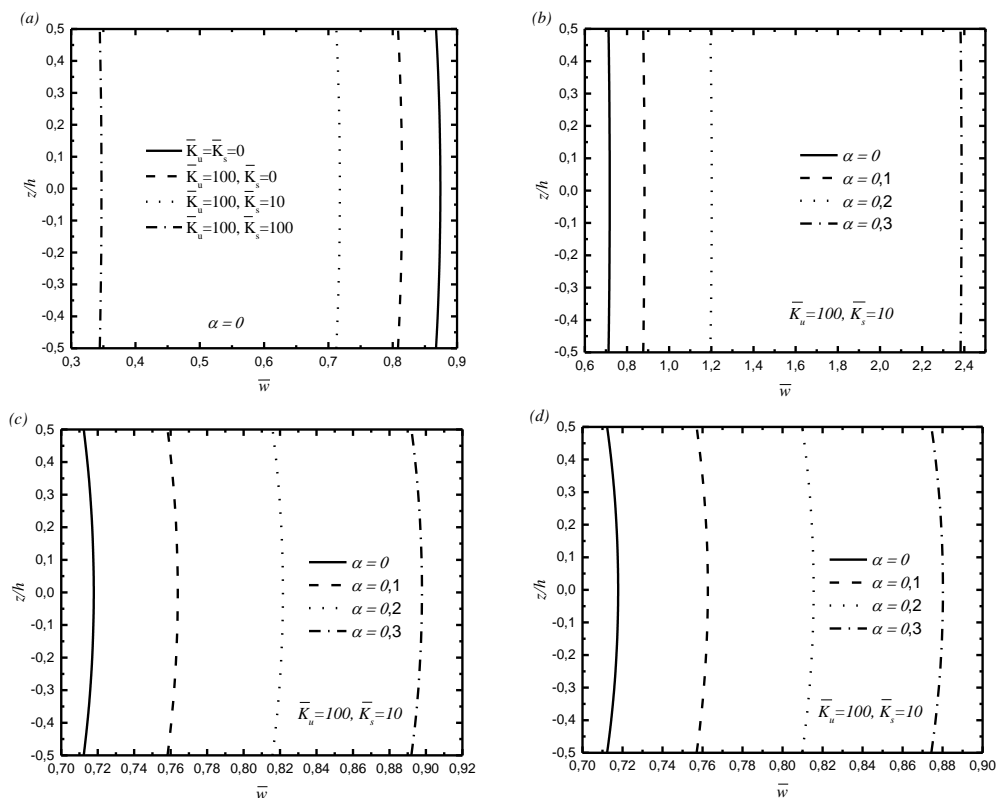
$(\bar{K}_w, \bar{G}_p)$	(a/h)	Perfect	Imperfect I (even)		Imperfect II (uneven)		Imperfect III (logarithmic-uneven)	
		$\alpha=0$	$\alpha=0.2$	$\alpha=0.5$	$\alpha=0.2$	$\alpha=0.5$	$\alpha=0.2$	$\alpha=0.5$
(0,0)	5	0.6397	0.8675	2.4657	0.6995	0.8243	0.6963	0.7976
	10	0.5695	0.7797	2.3254	0.6180	0.7173	0.6155	0.6963
	20	0.5518	0.7576	2.2899	0.5974	0.6903	0.5951	0.6707
(100,0)	5	0.5785	0.7585	1.7473	0.6269	0.7253	0.6244	0.7046
	10	0.5200	0.6897	1.6721	0.5601	0.6404	0.5580	0.6236
	20	0.5049	0.6719	1.6523	0.5428	0.6184	0.5409	0.6027
(100,100)	5	0.2001	0.2177	0.2584	0.2055	0.2149	0.2052	0.2130
	10	0.1913	0.2103	0.2554	0.1965	0.2054	0.1962	0.2037
	20	0.1886	0.2078	0.2544	0.1936	0.2024	0.1934	0.2007

Table 7 Non-dimensional deflection $\bar{w}$ of square isotropic and FG plates resting on Kerr foundation $(\bar{K}_l = 100)$

$\bar{K}_u$	$\bar{K}_s$	a/h	Isotropic plate		FG plate			
			Ceramic	Metal	p=0.5	p=1.0	p=2.0	p=5.0
100	0	20	0.277131	1.363622	0.416313	0.527335	0.658800	0.778160
		10	0.287172	1.409126	0.429470	0.543630	0.681242	0.814469
		5	0.326733	1.584470	0.481184	0.607582	0.769141	0.959577
100	100	20	0.189785	0.417700	0.246124	0.281089	0.314517	0.339377
		10	0.194842	0.423748	0.251300	0.286419	0.320423	0.347141
		5	0.213199	0.441534	0.269583	0.304953	0.340607	0.372736
200	100	20	0.170918	0.336057	0.215300	0.241581	0.265859	0.283409
		10	0.175123	0.340379	0.219420	0.245704	0.270285	0.289054
		5	0.190054	0.352272	0.233574	0.259616	0.284942	0.307042
200	200	20	0.123992	0.192678	0.145788	0.157371	0.167313	0.174101
		10	0.126414	0.194602	0.147957	0.159423	0.169379	0.176566
		5	0.134441	0.198825	0.154778	0.165710	0.175567	0.183642

Table 8 Variations of Non-dimensional stress $\bar{\sigma}_x(h/3)$ of perfect and imperfect FG square plates versus the Kerr foundation stiffness $(p = 1, \bar{K}_l = 100)$

$(\bar{K}_u, \bar{K}_s)$	a/h	Perfect	Imperfect I (even)		Imperfect II (uneven)		Imperfect III (logarithmic-uneven)	
		$\alpha = 0$	$\alpha = 0.2$	$\alpha = 0.5$	$\alpha = 0.2$	$\alpha = 0.5$	$\alpha = 0.2$	$\alpha = 0.5$
(100, 0)	20	2.794258	2.869319	3.541020	2.710523	2.529268	2.714962	2.568618
	10	1.395791	1.432925	1.767293	1.352675	1.259340	1.354961	1.279601
	5	0.694908	0.712684	0.876936	0.670874	0.618868	0.672148	0.630149
(100, 100)	20	1.489524	1.314269	0.844666	1.393629	1.213730	1.398478	1.250109
	10	0.736002	0.649063	0.418658	0.686925	0.594999	0.689407	0.613566
	5	0.352375	0.310496	0.203453	0.325913	0.276706	0.327249	0.286593
(200, 100)	20	1.280190	1.104625	0.666849	1.190994	1.026720	1.195476	1.059631
	10	0.631562	0.544821	0.330469	0.586028	0.502311	0.588315	0.519061
	5	0.300999	0.259829	0.160822	0.276675	0.232297	0.277894	0.241128
(200, 200)	20	0.834003	0.687288	0.370190	0.766648	0.647145	0.769990	0.670641
	10	0.410234	0.338304	0.183540	0.376041	0.315489	0.377736	0.327377
	5	0.194416	0.161145	0.090022	0.176474	0.144945	0.177362	0.151101

Fig. 2 Through-the-thickness distribution of $\bar{w}$ of isotropic FG non-porous and porous square plates resting on Kerr elastic foundations (a) for different parameters of foundations and for different porosity factor (a) Imperfect I (even), (c) Imperfect II (uneven) and (d) Imperfect III (logarithmic-uneven) (a=10 h, p=5, $\bar{K}_l = 100$)
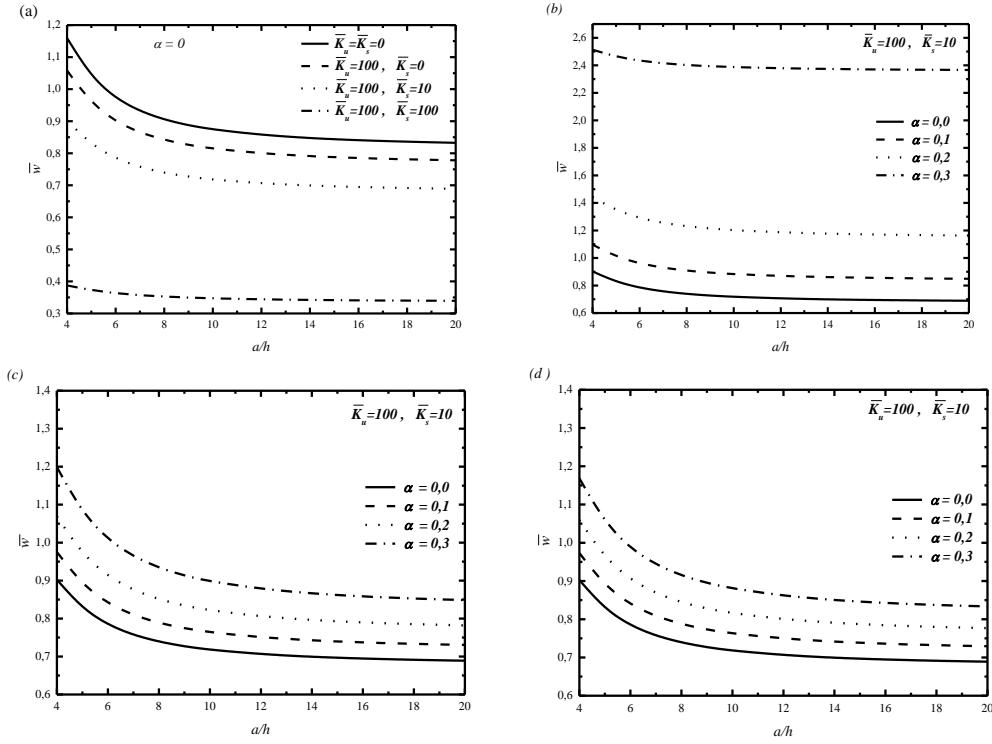
Fig. 3 Variation of $\bar{w}$ versus the side-to-thickness ratio *a/h* of FG non-porous and porous square plates resting on kerr foundations (a) for different parameters of foundations and for different porosity factor (b) Imperfect I (even), (c) Imperfect II (uneven) and (d) Imperfect III (logarithmic-uneven) (p=5, $\bar{K}_l = 100$)
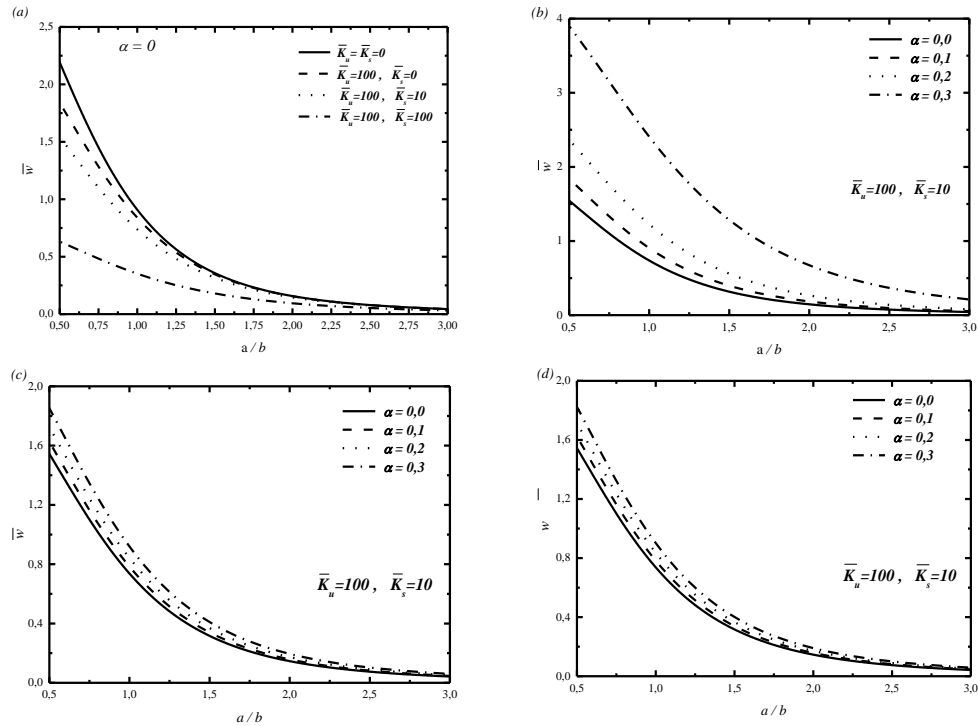

Fig. 4 Variation of $\bar{w}$ versus the aspect ratio *a/b* of FG non-porous and porous square plates resting on Kerr foundations (a) for different parameters of foundations and for different porosity factor (b) Imperfect I (even), (c) Imperfect II (uneven) and (d) Imperfect III (logarithmic-uneven) (a=10 h, p=5, $\bar{K}_l = 100$)

foundation stiffness ($p = 1, \bar{K}_l = 100$) is considered to study the influence of increasing porosity volume index. For the porous FG plate, three kinds of porosity distribution are investigated. Various length to thickness ratio and porosity parameter are presented. The results are listed in Table 8. It is noted that the non-dimensional stress of the
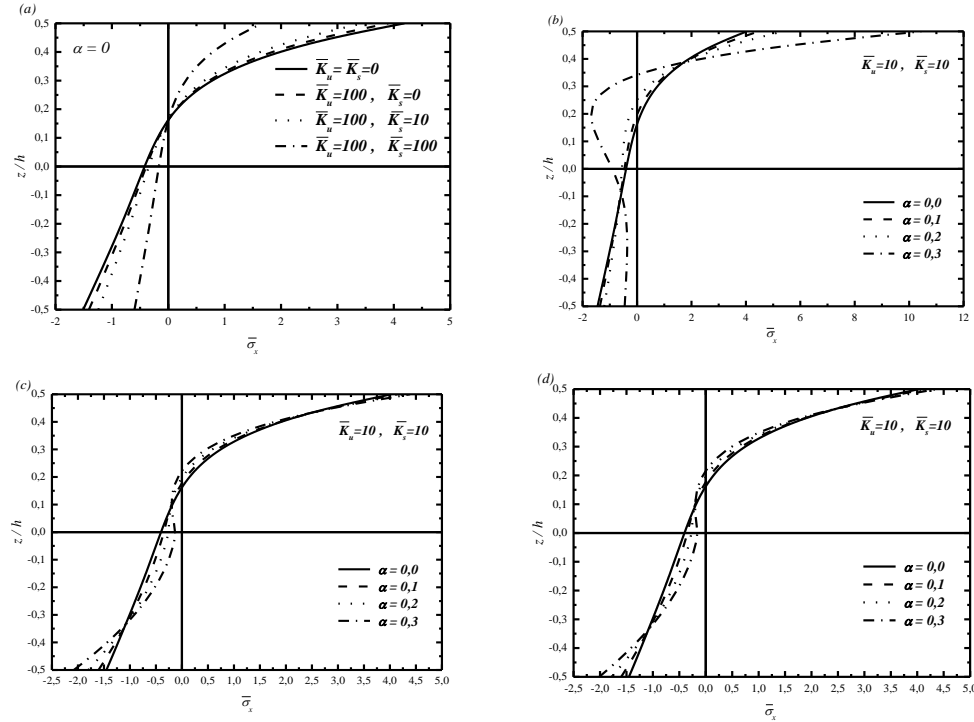
Fig. 5 In-plane normal stress $\bar{\sigma}_x$ through-the-thickness distributions of FG non-porous and porous square plates resting on Kerr foundation (a) for different parameters of foundations and for different porosity volume index (b) Imperfect I (even), (c) Imperfect II (uneven) and (d) Imperfect III (logarithmic-uneven) for different porosity volume index (a=10h, p=5, $\bar{K}_l = 100$)

Table 9 Non-dimensional natural frequencies $\hat{\omega} = \omega h\sqrt{\rho/G}$ of an isotropic square plate with v=0.3 and a/h=10

Model	Mode (m, n)						
	(1, 1)	(1, 2)	(2, 2)	(2, 3)	(3, 3)	(2, 4)	(1, 5)
Exact 3D (Zhou *et al.* 2002)	0.0932	0.2226	0.3421	0.5239	0.6889	0.7511	0.9268
Jha *et al.* (2013) $\varepsilon_z \neq 0$	0.0932	0.2226	0.3421	0.5240	0.6892	0.7515	0.9275
Akavci and Tanrikulu (2015) $\varepsilon_z \neq 0$	0.0932	0.2227	0.3424	0.5247	0.6902	0.7526	0.9290
Benahmed *et al.* (2017) $\varepsilon_z \neq 0$	0.0932	0.2229	0.3425	0.5248	0.6904	0.7528	0.9294
Farzam-Rad *et al.* (2017) $\varepsilon_z \neq 0$	0.0932	0.2227	0.3423	0.5243	0.6896	0.7520	0.9284
Shahsavari *et al.* (2018) $\varepsilon_z \neq 0$	0.0932	0.2226	0.3421	0.5240	0.6892	0.7514	0.9274
Present $\varepsilon_z \neq 0$	0.0932	0.2226	0.3421	0.5240	0.6891	0.7513	0.9273

plate FG decreases as the parameters of the upper layer ($\bar{K}_u$) and the shear layer ($\bar{K}_s$) of the spring increase. It is important to note that the shear layer parameter is more efficient than the other two parameters of the upper and lower layer ($\bar{K}_u, \bar{K}_l$). We note that for a logarithmic distribution of uneven porosity, the stress $\bar{\sigma}_x$ increases. The logarithmic function has a significant effect on high porosity volume indices and has no significant effect on low porosity volume indices. Also, it is important to point out that the Kerr elastic foundation plays an important role in imperfect FG plate responses.

As another verification attempt, it can seen that the fundamental frequencies $\bar{\omega}$ of FG plate embedded in Kerr foundation are bigger than those embedded in Winkler and Pasternak foundations due to an extra upper spring.

Fig. 2 shows the deflection $\bar{w}$ through-the-thickness of FG non-porous and porous square plates resting on Kerr foundations (a=10h, p=5, $\bar{K}_l = 100$). The deflection $\bar{w}$ decreases as as the parameters of the upper layer ($\bar{K}_u$) and the shear layer ($\bar{K}_s$) of the spring and porosity volume

fraction α increase.

Fig. 3 display the variations of the the non-dimensional deflection $\bar{w}$ versus the side-to-thickness ratio a/h of FG non-porous and porous plates resting on Kerr foundations (p=5, $\bar{K}_l = 100$). It is also observed that the deflection $\bar{w}$ decreases with increase two parametres ($\bar{K}_u, \bar{K}_s$), porosity volume fraction α and ratio a/h.

Fig. 4 illustrate the variations of the the non-dimensional deflection $\bar{w}$ as functions of the aspect ratio a/b of FG non-porous and porous plates resting on Kerr foundations (a=10h, p=5, $\bar{K}_l = 100$). It can be noticed that the $\bar{w}$ decreases with increase two parametres ($\bar{K}_u, \bar{K}_s$) and decrease directly as a/b increases, as shown in Fig. 4a. It can be noticed that when porosity volume fraction α increase, non-dimensional deflection $\bar{w}$ increase. Also, it observed that the deflection $\bar{w}$ for even porosité is bigger than an other distribution.

Fig. 5 displays the in-plane normal stress $\bar{\sigma}_x$ of FG non-porous and porous square plates through the thickness resting on Kerr foundations (a=10 h, p=5, $\bar{K}_l = 100$). The
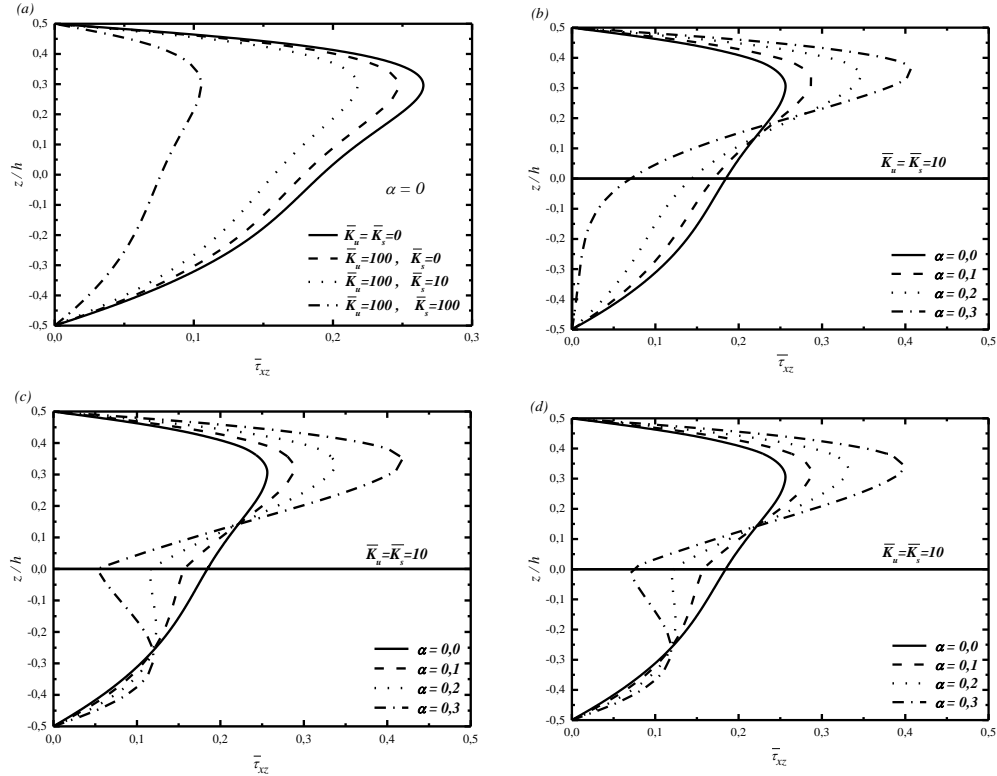
Fig. 6 The shear stress $\bar{\tau}_{xz}$ through-the-thickness distributions of FG non-porous and porous square plates resting on Kerr foundation (a) for different parameters of foundations and for different porosity volume index (b) Imperfect I (even), (c) Imperfect II (uneven) and (d) Imperfect III (logarithmic-uneven) for different porosity volume index ($a=10h$, $p=5$, $\bar{K}_l = 100$)

Table 10 Non-dimensional natural frequencies $\tilde{\omega} = \omega h \sqrt{\rho_m / E_m}$ of FG plate $\varepsilon_z \neq 0$

a/h	Model	$a/b = 0.5$			$a/b = 1$		
		$p = 0$	$p = 1$	$p = 2$	$p = 0$	$p = 1$	$p = 2$
2	Exact 3D (Jin *et al.* 2014)	0.9570	0.7937	0.7149	1.8470	1.4687	1.3095
	Mantari *et al.* (2014) $\varepsilon_z \neq 0$	1.3040	1.0346	0.9293	1.8505	1.4774	1.3219
	Farzam-Rad *et al.* (2017) $\varepsilon_z \neq 0$	0.9570	0.7961	0.7193	1.8528	1.4788	1.3226
	Shahsavari *et al.* (2018) $\varepsilon_z \neq 0$	1.3039	1.0345	0.9293	1.8503	1.4772	1.3218
	Present $\varepsilon_z \neq 0$	1.3038	1.0344	0.9292	1.8500	1.4770	1.3216
5	Exact 3D (Jin *et al.* 2014)	0.□713	0.2088	0.1888	0.4169	0.3222	0.2905
	Mantari *et al.* (2014) $\varepsilon_z \neq 0$	0.2712	0.2115	0.1926	0.4168	0.3260	0.2961
	Farzam-Rad *et al.* (2017) $\varepsilon_z \neq 0$	0.2714	0.2116	0.1926	0.4170	0.3262	0.2961
	Shahsavari *et al.* (2018) $\varepsilon_z \neq 0$	0.2712	0.2115	0.1926	0.4□68	0.3260	0.2961
	Present $\varepsilon_z \neq 0$	0.2712	0.2115	0.1926	0.4168	0.3260	0.2961
10	Exact 3D (Jin *et al.* 2014)	0.0719	0.0550	0.0499	0.1135	0.0870	0.0789
	Mantari *et al.* (2014) $\varepsilon_z \neq 0$	0.0718	0.0557	0.0510	0.1135	0.0882	0.0806
	Farzam-Rad *et al.* (2017) $\varepsilon_z \neq 0$	0.0719	0.0558	0.0510	0.1136	0.0882	0.0806
	Shahsavari *et al.* (2018) $\varepsilon_z \neq 0$	0.0718	0.0557	0.0510	0.1135	0.0882	0.0806
	Present $\varepsilon_z \neq 0$	0.0718	0.0557	0.0510	0.1135	0.0882	0.0806

tensile stress $\bar{\sigma}_x$ increases along the lower half-plane by increasing the two parametres ($\bar{K}_u$, $\bar{K}_s$) and is increase with the increase of the porosity volume fraction α. But, the tensile in-plane normal stress $\bar{\sigma}_x$ decrease along the upper half-plane by increasing the two parametres ($\bar{K}_u$, $\bar{K}_s$).

Fig. 6 shows the shear stress $\bar{\tau}_{xz}$ in FG non-porous and porous plates through-the-thickness for different values of the foundation stiffnesses ($\bar{K}_u$, $\bar{K}_s$) and the porosity volume fraction α, respectively ($a=10h$, $p=5$, $\bar{K}_l = 100$). One can note that the shear stress $\bar{\tau}_{xz}$ decreases by increasing the foundation stiffnesses ($\bar{K}_u$, $\bar{K}_s$) and increases in $0.2h \leq z \leq 0.5h$ and decreases in $-0.5h \leq z \leq 0.2h$ by increasing the porosity volume fraction α.

4.2 Results of vibration analysis

Table 9 shows the non-dimensional natural frequencies

Table 11 Non-dimensional fundamental frequencies $\tilde{\omega} = \omega\, h\sqrt{\rho_m / E_m}$ of square isotropic and FG plates resting on Winkler-Pasternak foundations

$\bar{K}_w$	$\bar{G}_p$	a/h	Model	p				
				0	0.5	1	2	5
0	0	20	Benahmed *et al*. (2017) $\varepsilon_z \neq 0$	0.0291	-	0.0226	0.0207	-
			Baferani *et al*. (2011) $\varepsilon_z = 0$	0.0290	0.0249	0.0227	0.0209	0.0197
			Shahsavari *et al*. (2018) $\varepsilon_z \neq 0$	0.0291	0.0248	0.0226	0.0206	0.0195
			Present $\varepsilon_z \neq 0$	0.0291	0.0248	0.0226	0.0206	0.0195
		10	Benahmed *et al*. (2017) $\varepsilon_z \neq 0$	0.1136	-	0.0883	0.0807	-
			Baferani *et al*. (2011)	0.1134	0.0975	0.0891	0.0819	0.0767
			Shahsavari *et al*. (2018) $\varepsilon_z \neq 0$	0.1135	0.0970	0.0882	0.0806	0.0755
			Present $\varepsilon_z \neq 0$	0.1135	0.0970	0.0882	0.0806	0.0755
		5	Benahmed *et al*. (2017) $\varepsilon_z \neq 0$	0.4174	-	0.3264	0.2965	-
			Baferani *et al*. (2011)	0.4154	0.3606	0.3299	0.3016	0.2765
			Shahsavari *et al*. (2018) $\varepsilon_z \neq 0$	0.4168	0.3586	0.3260	0.2961	0.2722
			Present $\varepsilon_z \neq 0$	0.4168	0.3586	0.3260	0.2961	0.2722
100	0	20	Benahmed *et al*. (2017) $\varepsilon_z \neq 0$	0.0298	-	0.0236	0.0218	-
			Baferani *et al*. (2011)	0.0298	0.0258	0.0238	0.0221	0.0210
			Shahsavari *et al*. (2018) $\varepsilon_z \neq 0$	0.0298	0.0257	0.0236	0.0218	0.0208
			Present $\varepsilon_z \neq 0$	0.0298	0.0257	0.0236	0.0218	0.0208
		10	Benahmed *et al*. (2017) $\varepsilon_z \neq 0$	0.1164	-	0.0924	0.0854	-
			Baferani *et al*. (2011)	0.1162	0.1012	0.0933	0.0867	0.0821
			Shahsavari *et al*. (2018) $\varepsilon_z \neq 0$	0.1163	0.1006	0.0923	0.0853	0.0809
			Present $\varepsilon_z \neq 0$	0.1163	0.1006	0.0923	0.0853	0.0809
		5	Benahmed *et al*. (2017) $\varepsilon_z \neq 0$	0.4286	-	0.3431	0.3158	-
			Baferani *et al*. (2011)	0.4273	0.3758	0.3476	0.3219	0.2999
			Shahsavari *et al*. (2018) $\varepsilon_z \neq 0$	0.4284	0.3734	0.3431	0.3159	0.2950
			Present $\varepsilon_z \neq 0$	0.4282	0.3731	0.3428	0.3155	0.2946
100	100	20	Benahmed *et al*. (2017) $\varepsilon_z \neq 0$	0.0411	-	0.0386	0.0383	-
			Baferani *et al*. (2011)	0.0411	0.0395	0.0388	0.0386	0.0388
			Shahsavari *et al*. (2018) $\varepsilon_z \neq 0$	0.0411	0.0393	0.0386	0.0383	0.0385
			Present $\varepsilon_z \neq 0$	0.0410	0.0393	0.0386	0.0383	0.0385
		10	Benahmed *et al*. (2017) $\varepsilon_z \neq 0$	0.1614	-	0.1521	0.1509	-
			Baferani *et al*. (2011)	0.1619	0.1563	0.1542	0.1535	0.1543
			Shahsavari *et al*. (2018) $\varepsilon_z \neq 0$	0.1616	0.1551	0.1525	0.1512	0.1521
			Present $\varepsilon_z \neq 0$	0.1613	0.1548	0.1521	0.1509	0.1517
		5	Benahmed *et al*. (2017) $\varepsilon_z \neq 0$	0.6089	-	0.5794	0.5752	-
			Baferani *et al*. (2011)	0.6162	0.6026	0.5978	0.5970	0.5993
			Shahsavari *et al*. (2018) $\varepsilon_z \neq 0$	0.6137	0.5940	0.5856	0.5815	0.5843
			Present $\varepsilon_z \neq 0$	0.6101	0.5898	0.5811	0.5769	0.5792

of a simply supported homogeneous square plate for $a/h = 10$ using the present theory. The present solutions which takes into account both the transverse shear and transverse normal deformation are compared to those obtained by Zhou *et al*. 2002 based on three-dimensional elasticity solutions and those given by the quasi-3D shear deformation theories by Jha *et al*. 2013, Akavci and Tanrikulu 2015, Benahmed *et al*. 2017, Farzam-Rad *et al*. 2017 and Shahsavari *et al*. 2018. Good agreement is achieved between the present solution and the published ones.

Also, comparison of non-dimensional natural frequencies is achieved in table 10 for various values of the ratios a/b and a/h. Excellent correlation is observed between the fundamental frequency obtained from the present study and that of exact 3D (Jin *et al*. 2014) and quasi-3D (Mantari *et al*. 2014, Farzam-Rad *et al*. 2017 and Shahsavari *et al*. 2018) results.

The non-dimensional natural frequency $\bar{\omega}$ of isotropic and FG plates versus the shear and Winkler parameters,

power law index p and thickness-length ratio a/h are listed in Table 11. These results are predicted by the shear and normal deformation theory which takes in account the stretching effect as well as theories of Refs (Benahmed *et al*. 2017, Shahsavari *et al*. 2018). It is obvious that the current results concerning the non-dimensional fundamental frequency of the FG plates integrated into the Winkler - Pasternak foundations are almost identical.

Table 12 exhibit the effects of the elastic foundation parameters $(\bar{K}_w, \bar{G}_p)$ and side-tothickness ratio *a/h* on the natural frequencies $\bar{\omega}$. For this, three types of pore distribution were considered, uniform distribution of porosities (FGM I), unequal distribution of porosities (FGM II) and imperfect materials with logarithm unequal distribution of porosities (FGM III). It is clear that for uneven porosity distributions the natural frequencies $\bar{\omega}$ increase with the increase of the porosity volume fraction α without or with elastic foundation and natural frequencies $\bar{\omega}$ increase when *a/h* increase. In addition, natural frequencies $\bar{\omega}$ increase with the existence of the elastic

Table 12 Variations of frequency parameters $\bar{\omega}$ of perfect and imperfect FG square plates versus the Winkler-Pasternak foundation stiffness (p=1)

$(\bar{K}_w, \bar{G}_p)$	a/h	Model	Perfect	Imperfect I (even)		Imperfect II (uneven)		Imperfect III (logarithmic-uneven)	
			$\alpha = 0$	$\alpha = 0.2$	$\alpha = 0.5$	$\alpha = 0.2$	$\alpha = 0.5$	$\alpha = 0.2$	$\alpha = 0.5$
(0, 0)	20	Shahsavari *et al.* (2018)	9.020	8.370	5.738	9.052	9.117	9.050	9.106
		Present $\varepsilon_z \neq 0$	9.020	8.370	5.738	9.051	9.116	9.053	9.105
	10	Shahsavari *et al.* (2018)	8.818	8.203	5.659	8.845	8.896	8.843	8.889
		Present $\varepsilon_z \neq 0$	8.818	8.203	5.659	8.842	8.895	8.859	8.887
	5	Shahsavari *et al.* (2018)	8.151	7.641	5.378	8.164	8.178	8.163	8.178
		Present $\varepsilon_z \neq 0$	8.151	7.641	5.378	8.153	8.177	8.225	8.177
(100, 0)	20	Shahsavari *et al.* (2018)	9.430	8.917	6.933	9.505	9.655	9.501	9.626
		Present $\varepsilon_z \neq 0$	9.429	8.917	6.933	9.503	9.653	9.504	9.624
	10	Shahsavari *et al.* (2018)	9.231	8.753	6.850	9.301	9.438	9.298	9.412
		Present $\varepsilon_z \neq 0$	9.228	8.750	6.848	9.296	9.434	9.312	9.408
	5	Shahsavari *et al.* (2018)	8.577	8.203	6.559	8.636	8.738	8.632	8.719
		Present $\varepsilon_z \neq 0$	8.569	8.196	6.553	8.617	8.729	8.709	8.711
(100, 100)	20	Shahsavari *et al.* (2018)	15.439	16.320	18.625	16.011	17.098	15.982	16.800
		Present $\varepsilon_z \neq 0$	15.430	16.313	18.621	16.002	17.089	15.975	16.871
	10	Shahsavari *et al.* (2018)	15.245	16.148	18.464	15.812	16.883	15.783	16.668
		Present $\varepsilon_z \neq 0$	15.211	16.118	18.446	15.777	16.850	15.758	16.635
	5	Shahsavari *et al.* (2018)	14.640	15.595	17.872	15.192	16.221	15.164	16.016
		Present $\varepsilon_z \neq 0$	14.528	15.477	17.731	15.073	16.100	15.080	15.896

Table 13 Non-dimensional fundamental frequencies $\bar{\omega}$ of square isotropic and FG plates resting on Kerr foundation ($\bar{K}_l = 100$)

| $\bar{K}_u$	$\bar{K}_s$	a/h	Model	Isotropic plate		FG plate			
				Ceramic	Metal	$p = 0.5$	$p = 1.0$	$p = 2.0$	$p = 5.0$
100	0	20	Shahsavari *et al.* (2018)	0.0294	0.0157	0.0253	0.0231	0.0212	0.0202
			Present $\varepsilon_z \neq 0$	0.0294	0.0158	0.0253	0.0231	0.0212	0.0202
		10	Shahsavari *et al.* (2018)	0.1149	0.0615	0.0988	0.0903	0.0830	0.0783
			Present $\varepsilon_z \neq 0$	0.1149	0.0624	0.0988	0.0903	0.0830	0.0782
		5	Shahsavari *et al.* (2018)	0.4226	0.2278	0.3661	0.3347	0.3061	0.2838
			Present $\varepsilon_z \neq 0$	0.4225	0.2375	0.3659	0.3345	0.3060	0.2836
100	100	20	Shahsavari *et al.* (2018)	0.0356	0.0285	0.0329	0.0316	0.0308	0.0305
			Present $\varepsilon_z \neq 0$	0.0356	0.0285	0.0329	0.0316	0.0307	0.0305
		10	Shahsavari *et al.* (2018)	0.1396	0.1125	0.1294	0.1245	0.1212	0.1201
			Present $\varepsilon_z \neq 0$	0.1395	0.1137	0.1292	0.1243	0.1210	0.1198
		5	Shahsavari *et al.* (2018)	0.5246	0.4332	0.4906	0.4739	0.4615	0.4560
			Present $\varepsilon_z \neq 0$	0.5226	0.4492	0.4883	0.4714	0.4589	0.4531
200	100	20	Shahsavari *et al.* (2018)	0.0375	0.0317	0.0351	0.0341	0.0335	0.0334
			Present $\varepsilon_z \neq 0$	0.0375	0.0318	0.0351	0.0341	0.0334	0.0334
		10	Shahsavari *et al.* (2018)	0.1473	0.1255	0.1385	0.1345	0.1320	0.1316
			Present $\varepsilon_z \neq 0$	0.1471	0.1269	0.1382	0.1342	0.1317	0.1313
		5	Shahsavari *et al.* (2018)	0.5559	0.4850	0.5273	0.5139	0.5047	0.5024
			Present $\varepsilon_z \neq 0$	0.5533	0.5026	0.5243	0.5107	0.5014	0.4988
200	200	20	Shahsavari *et al.* (2018)	0.0440	0.0419	0.0427	0.0423	0.0422	0.0426
			Present $\varepsilon_z \neq 0$	0.0440	0.0420	0.0427	0.0422	0.0422	0.0426
		10	Shahsavari *et al.* (2018)	0.1735	0.1660	0.1687	0.1670	0.1668	0.1684
			Present $\varepsilon_z \neq 0$	0.1731	0.1678	0.1683	0.1666	0.1663	0.1680
		5	Shahsavari *et al.* (2018)	0.6617	0.5511	0.6484	0.6436	0.6431	0.6494
			Present $\varepsilon_z \neq 0$	0.6572	0.5511	0.6431	0.6380	0.6372	0.6430

foundations. The inclusion of the Pasternak's foundation parameters gives results more than those with the inclusion of Winkler's foundation parameter

Table 13 exhibit the effects of the Kerr foundation parameters $(\bar{K}_u, \bar{K}_s)$, volume fraction indices p and side-to-thickness ratio a/h on the fundamental frequencies $\bar{\omega}$ of square isotropic and FG plates resting on Kerr foundation ($\bar{K}_l = 100$) on the basis of the present quasi-3D shear deformation plate theories. As it can be seen, that upper spring and shear layer parameter have rising effects. The

Table 14 Variations of frequency parameters $\bar{\omega}$ of perfect and imperfect FG square plates versus the Kerr foundation stiffness ($p = 1, \bar{K}_l = 100$)

$(\bar{K}_u, \bar{K}_s)$	a/h	Model	Perfect	Imperfect I (even)		Imperfect II (uneven)		Imperfect III (logarithmic-uneven)	
			$\alpha = 0$	$\alpha = 0.2$	$\alpha = 0.5$	$\alpha = 0.2$	$\alpha = 0.5$	$\alpha = 0.2$	$\alpha = 0.5$
(100, 0)	20	Shahsavari *et al.* (2018)	9.227	8.648	6.364	9.281	9.390	9.278	9.369
		Present $\varepsilon_z \neq 0$	9.227	8.648	6.363	9.280	9.388	9.281	9.368
	10	Shahsavari *et al.* (2018)	9.027	8.482	6.282	9.076	9.171	9.073	9.154
		Present $\varepsilon_z \neq 0$	9.026	8.481	6.282	9.072	9.169	9.089	9.151
	5	Shahsavari *et al.* (2018)	8.367	7.927	5.997	8.403	8.462	8.401	8.453
		Present $\varepsilon_z \neq 0$	8.363	7.923	5.994	8.388	8.457	8.457	8.448
(100,100)	20	Shahsavari *et al.* (2018)	12.643	12.969	13.780	13.006	13.702	12.987	13.562
		Present $\varepsilon_z \neq 0$	12.638	12.965	13.778	12.999	13.696	12.984	13.556
	10	Shahsavari *et al.* (2018)	12.454	12.807	13.656	12.811	13.494	12.793	13.357
		Present $\varepsilon_z \neq 0$	12.433	12.789	13.646	12.789	13.474	12.783	13.337
	5	Shahsavari *et al.* (2018)	11.849	12.281	13.216	12.196	12.847	12.178	12.718
		Present $\varepsilon_z \neq 0$	11.786	12.218	13.153	12.126	12.780	12.164	12.651
(200,100)	20	Shahsavari *et al.* (2018)	13.639	14.174	15.564	14.079	14.920	14.056	14.751
		Present $\varepsilon_z \neq 0$	13.632	14.169	15.561	14.072	14.913	14.052	14.744
	10	Shahsavari *et al.* (2018)	13.449	14.009	15.426	13.884	14.710	13.862	14.545
		Present $\varepsilon_z \neq 0$	13.423	13.987	15.414	13.857	14.686	13.846	14.520
	5	Shahsavari *et al.* (2018)	12.847	13.477	14.934	13.270	14.063	13.249	13.905
		Present $\varepsilon_z \neq 0$	12.767	13.395	14.847	13.183	13.977	13.209	13.820
(200,200)	20	Shahsavari *et al.* (2018)	16.901	18.040	21.010	17.575	18.851	17.541	18.595
		Present $\varepsilon_z \neq 0$	16.890	18.032	21.006	17.564	18.841	17.532	18.584
	10	Shahsavari *et al.* (2018)	16.704	17.861	20.832	17.372	18.630	17.338	18.377
		Present $\varepsilon_z \neq 0$	16.662	17.825	20.807	17.330	18.589	17.304	18.337
	5	Shahsavari *et al.* (2018)	16.089	17.286	20.147	16.739	17.947	16.706	17.706
		Present $\varepsilon_z \neq 0$	15.950	17.136	19.956	16.592	17.795	16.587	17.556
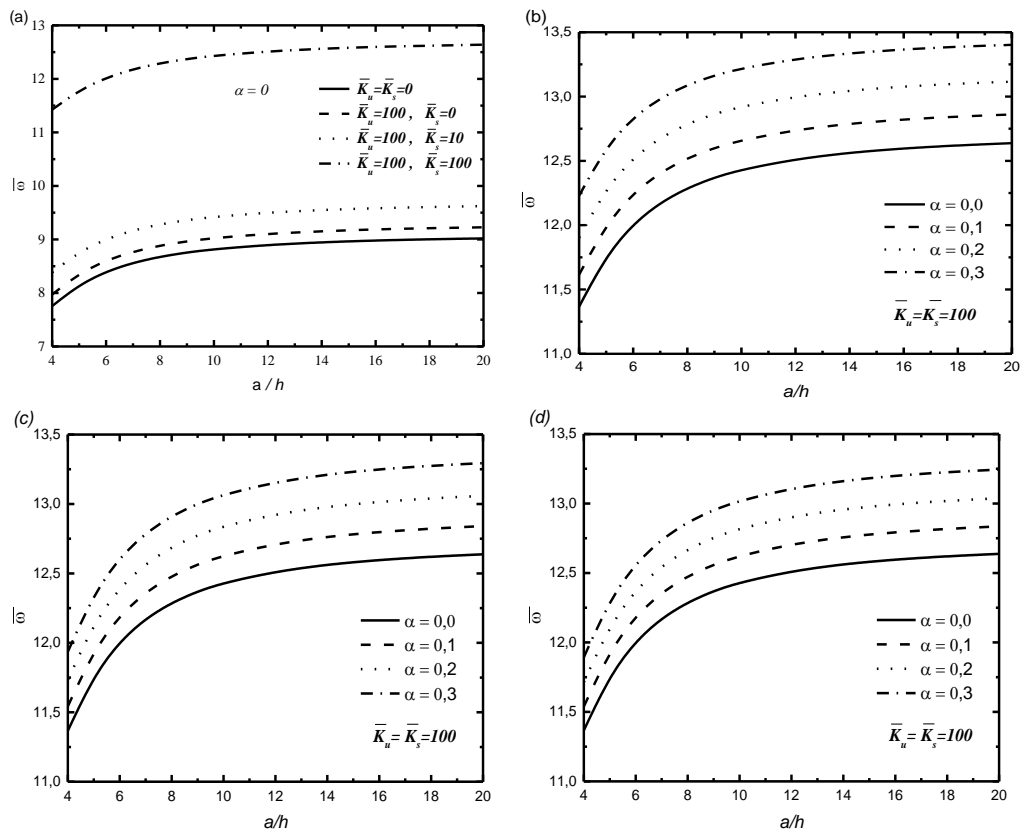
Fig. 7 Free vibration $\bar{\omega}$ versus the ratio *a/h* of FG non-porous and porous square plates resting on kerr foundations (a) for different parameters of foundations and for different porosity factor (b) Imperfect I (even), (c) Imperfect II (uneven) and (d) Imperfect III (logarithmic-uneven) (*p*=1, $\bar{K}_l = 100$)
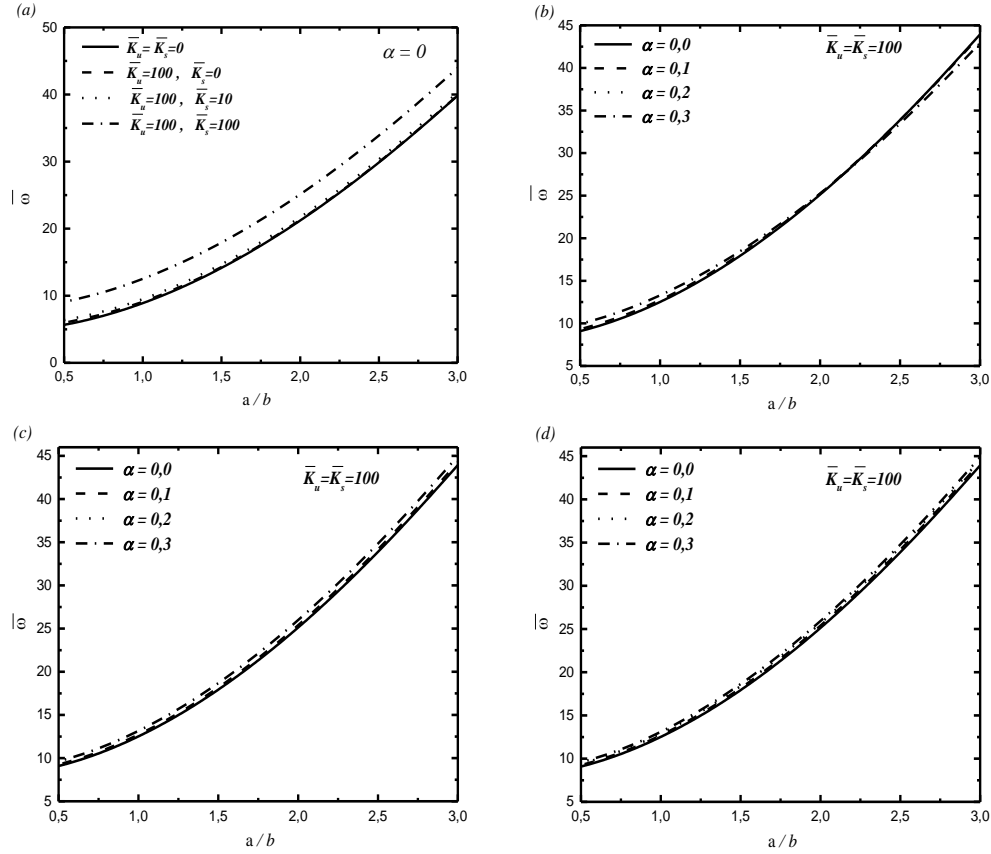
Fig. 8 Free vibration $\overline{\omega}$ versus the aspect ratio *a/b* of FG non-porous and porous square plates resting on Kerr foundations (a) for different parameters of foundations and for different porosity factor (b) Imperfect I (even), (c) Imperfect II (uneven) and (d) Imperfect III (logarithmic-uneven) (*p*=1, $\overline{K}_l = 100$)

shear parameter has more effect than the lower and upper spring constants.

The variations of frequency parameters $\overline{\omega}$ of nonporous and porous FG square plates versus the Kerr foundation stiffness ($p = 1, \overline{K}_l = 100$) is considered to study the influence of increasing porosity volume index. For the porous FG plate, three kinds of porosity distribution are investigated. Various length to thickness ratio and porosity parameter are presented. The results are listed in Table 14. It is noted that the frequency parameters $\overline{\omega}$ of the plate FG increases as the parameters of the upper layer ($\overline{K}_u$) and the shear layer ($\overline{K}_s$) of the spring increase. It is important to note that the shear layer parameter is more efficient than the other two parameters of the upper and lower layer ($\overline{K}_u, \overline{K}_l$). Table 14 shows the influence of the porosity volume index for the various porosity distribution models in a simply supported FG plate resting on a Kerr-type elastic foundation. We note that for a logarithmic distribution of uneven porosity, the frequency $\overline{\omega}$ decreases. The logarithmic function has a significant effect on high porosityvolume indices and has no significant effect on low porosity volume indices. Also, it is important to point out that the Kerr elastic foundation plays an important role in imperfect FG plate responses.

The non-dimensional fundamental natural frequency $\overline{\omega}$ of simply supported square FG plates resting on Kerr foundation ($\overline{K}_l = 100$) for various values of side-to

thickness ratios *a/h* is plotted in Fig. 7 based on the present new quasi-3D hyperbolic shear deformation theory. As can be seen, the frequency decreases significantly with the increase elastic foundation parameters ($\overline{K}_u, \overline{K}_s$) and porosity volume index.

Fig. 8 illustrate the variations of the natural frequencies $\overline{\omega}$ as functions of the aspect ratio *a/b* of simply supported square FG plates resting on Kerr foundation ($\overline{K}_l = 100, p = 1$) for various values of the elastic foundation parameters ($\overline{K}_u, \overline{K}_s$) and porosity volume index. It is noted that the frequency parameters $\overline{\omega}$ of the plate FG increases as the parameters of the upper layer ($\overline{K}_u$) and the shear layer ($\overline{K}_s$) of the spring increase. The frequencies increase directly as a/b increases and porosity volume index.

5. Conclusions

A novel quasi-3D hyperbolic shear deformation theory for bending and free vibration analysis of FG porous plates resting on elastic foundations is proposed in this paper. It contains only five unknowns, accounts for a hyperbolic distribution of transverse shear stress and satisfies the traction free boundary conditions. Equations of motion derived from the Hamilton principle are analytically solved for bending and free vibration problems of a simply supported plate. Benchmark comparisons of the solutions

obtained for a degradation model with ones in literature are conducted to verify the accuracy and efficiency of the present theory. The following main points may be drawn from the present study:

(1) Comparative studies reveal that the present theory is not only accurate, but also more efficient since the number of unknown functions involved in the present theory is only five, compared with other theories containing six or more unknown functions.

(2) The effects of shear and Winkler parameters, power law index p and thickness-length ratio a/h in bending and free vibration analysis. These results are predicted by the shear and normal deformation theory which takes in account the stretching effect. It is obvious that the current results of the FG plates integrated into the Winkler - Pasternak foundations are almost identical.

(3) The influence of the effect of normal deformation (stretching effect) on the performance of imperfect plates containing porosities are in good agreement for all cases.

(4) The effects of the Kerr foundation parameters, volume fraction indices p and side-to-thickness ratio a/h on bending and free vibration is analysis, then we seen that the non-dimensional deflection $\bar{w}$ of FG plate embedded in Kerr foundation are small than those embedded in Winkler and Pasternak foundations due to an extra upper spring while fundamental frequencies $\bar{\omega}$ is reversed.

An improvement of the present formulation will be considered in the future work to consider other type of materials (Hirwani *et al.* 2016b, Keikha *et al.* 2018, Al-Osta 2019, Fadoun 2019, Rajabi and Mohammadimehr 2019, Kunche *et al.* 2019).

References

Abrate, S. (2008), "Functionally graded plates behave like homogeneous plates", *Compos. Part B: Eng.*, **39**(1), 151-158. https://doi.org/10.1016/j.compositesb.2007.02.026.

Adim, B. and Daouadji, T.H. (2016), "Effects of thickness stretching in FGM plates using a quasi-3D higher order shear deformation theory", *Adv. Mater. Res.*, **5**(4), 223-244. https://doi.org/10.12989/amr.2016.5.4.223.

Akavci, S. and Tanrikulu, A. (2015), "Static and free vibration analysis of functionally graded plates based on a new quasi-3D and 2D shear deformation theories", *Compos. Part B: Eng.*, **83**, 203-215. https://doi.org/10.1016/j.compositesb.2015.08.043.

Akbaş, Ş.D. (2015), "Wave propagation of a functionally graded beam in thermal environments", *Steel Compos. Struct.*, **19**(6), 1421-1447. http://dx.doi.org/10.12989/scs.2015.19.6.1421.

Al-Osta, M.A. (2019), "Shear behaviour of RC beams retrofitted using UHPFRC panels epoxied to the sides", *Comput. Concrete*, **24**(1), 37-49. https://doi.org/10.12989/cac.2019.24.1.037.

Amar, L.H.H., Kaci, A. and Tounsi, A. (2017), "On the size-dependent behavior of functionally graded micro-beams with porosities", *Struct. Eng. Mech.*, **64**(5), 527-541. https://doi.org/10.12989/sem.2017.64.5.527.

Amar, L.H.H., Kaci, A., Yeghnem, R. and Tounsi, A. (2018), "A new four-unknown refined theory based on modified couple stress theory for size-dependent bending and vibration analysis of functionally graded micro-plate", *Steel Compos. Struct.*,

26(1), 89-102. https://doi.org/10.12989/scs.2018.26.1.089.

Arefi M. (2015), "Elastic solution of a curved beam made of functionally graded materials with different cross sections", *Steel Compos. Struct.*, **18**(3), 659-672. http://dx.doi.org/10.12989/scs.2015.18.3.659.

Arefi, M. (2015), "The effect of different functionalities of FGM and FGPM layers on free vibration analysis of the FG circular plates integrated with piezoelectric layers", *Smart Struct. Syst.*, **15**(5), 1345-1362. http://dx.doi.org/10.12989/sss.2015.15.5.1345.

Avcar, M. (2019), "Free vibration of imperfect sigmoid and power law functionally graded beams", *Steel Compos. Struct.*, **30**(6), 603-615. https://doi.org/10.12989/scs.2019.30.6.603.

Baferani, A.H., Saidi, A. and Ehteshami, H. (2011), "Accurate solution for free vibration analysis of functionally graded thick rectangular plates resting on elastic foundation", *Compos. Struct.*, **93**(7), 1842-1853. https://doi.org/10.1016/j.compstruct.2011.01.020.

Belkacem, A., Tahar, H.D., Abderrezak, R., Amine, B. M., Mohamed, Z. and Boussad, A. (2018), "Mechanical buckling analysis of hybrid laminated composite plates under different boundary conditions", *Struct. Eng. Mech.*, **66**(6), 761-769. https://doi.org/10.12989/sem.2018.66.6.761.

Bensaid, I. (2017), "A refined nonlocal hyperbolic shear deformation beam model for bending and dynamic analysis of nanoscale beams", *Adv. Nano Res.*, **5**(2), 113-126. https://doi.org/10.12989/anr.2017.5.2.113.

Bisen, H.B., Hirwani, C.K., Satankar, R.K., Panda, S.K., Mehar, K. and Patel, B. (2018), "Numerical study of frequency and deflection responses of natural fiber (Luffa) reinforced polymer composite and experimental validation", *J. Nat. Fib.*, 1-15. https://doi.org/10.1080/15440478.2018.1503129.

Bouguenina, O., Belakhdar, K., Tounsi, A. and Adda Bedia, E.A. (2015), "Numerical analysis of FGM plates with variable thickness subjected to thermal buckling". *Steel Compos. Struct.,* **19**(3), 679-695. http://dx.doi.org/10.12989/scs.2015.19.3.679.

Carrera, E., Brischetto, S., Cinefra, M. and Soave, M. (2011). "Effects of thickness stretching in functionally graded plates and shells", *Compos.: Part B.*, **42**, 123-133. https://doi.org/10.1016/j.compositesb.2010.10.005.

Carrera, E., Brishetto, S. and RRobaldo, A. (2008), "Variable kinematic model for the analysis of functionally graded material plates", *AIAA J.*, **46**, 194-203. https://doi.org/10.2514/1.32490.

Chandra Mouli, B., Ramji, K., Kar, V.R., Panda, S.K., Lalepalli, A.K. and Pandey, H.K. (2018), "Numerical study of temperature dependent eigenfrequency responses of tilted functionally graded shallow shell structures", *Struct. Eng. Mech.*, **68**(5), 527-536. https://doi.org/10.12989/sem.2018.68.5.527.

Čukanović, D., Radaković, A., Bogdanović, G., Milanović, M., Redžović, H. and Dragović, D. (2018), "New shape function for the bending analysis of functionally graded plate", *Mater.*, **11**(12), 2381. https://doi.org/10.3390/ma11122381.

Darilmaz, K. (2015), "Vibration analysis of functionally graded material (FGM) grid systems", *Steel Compos. Struct.*, **18**(2), 395-408. https://doi.org/10.12989/scs.2015.18.2.395.

Ebrahimi, F. and Dashti, S. (2015), "Free vibration analysis of a rotating non-uniform functionally graded beam", *Steel Compos. Struct.*, **19**(5), 1279-1298. https://doi.org/10.12989/scs.2015.19.5.1279.

Ebrahimi, F. and Habibi, S. (2016), "Deflection and vibration analysis of higher-order shear deformable compositionally graded porous plate", *Steel Compos. Struct.*, **20**(1), 205-225. http://dx.doi.org/10.12989/scs.2016.20.1.205.

Ehyaei, J., Akbarshahi, A. and Shafiei, N. (2017), "Influence of porosity and axial preload on vibration behavior of rotating FG nanobeam", *Adv. Nano Res.*, **5**(2), 141-169. https://doi.org/10.12989/anr.2017.5.2.141.

Fadoun, O.O. (2019), "Analysis of axisymmetric fractional

vibration of an isotropic thin disc in finite deformation", *Comput. Concrete*, **23**(5), 303-309. https://doi.org/10.12989/cac.2019.23.5.303.

Faleh, N.M., Ahmed, R.A. and Fenjan, R.M. (2018), "On vibrations of porous FG nanoshells", *Int. J. Eng. Sci.*, **133**, 1-14. https://doi.org/10.1016/j.ijengsci.2018.08.007.

Farzam-Rad, S.A., Hassani, B. and Karamodin, A. (2017), "Isogeometric analysis of functionally graded plates using a new quasi-3D shear deformation theory based on physical neutral surface", *Compos.: Part B Eng.*, **108**, 174-189. https://doi.org/10.1016/j.compositesb.2016.09.029.

Ferreira, A.J.M., Castro, L.M. and Bertoluzza, S. (2009), "A high order collocation method for the static and vibration analysis of composite plates using a first-order theory", *Compos. Struct.*, **89**(3), 424-432. https://doi.org/10.1016/j.compstruct.2008.09.006.

Hadji, L., Meziane, M.A.A. and Safa, A. (2018), "Mechanical behaviour of FGM sandwich plates using a quasi-3D higher order shear and normal deformation theory", *Struct. Eng. Mech.*, **66**(6), 771-781. https://doi.org/10.12989/sem.2017.61.1.049.

Hebali, H., Tounsi, A., Houari, M.S.A., Bessaim, A. and Bedia, E.A.A. (2014), "New quasi-3D hyperbolic shear deformation theory for the static and free vibration analysis of functionally graded plates", *J. Eng. Mech.*, **140**(2), 374-383. https://doi.org/10.1061/(ASCE)EM.1943-7889.0000665.

Hirwani, C.K. and Panda, S.K. (2018), "Numerical and experimental validation of nonlinear deflection and stress responses of pre-damaged glass-fibre reinforced composite structure", *Ocean Eng.*, **159**, 237-252. https://doi.org/10.1016/j.oceaneng.2018.04.035.

Hirwani, C.K., Panda, S.K. and Patel, B.K. (2018c), "Theoretical and experimental validation of nonlinear deflection and stress responses of an internally debonded layer structure using different higher-order theories", *Acta Mechanica*, **229**(8), 3453-3473. https://doi.org/10.1007/s00707-018-2173-8.

Hirwani, C.K., Panda, S.K., Mahapatra, S.S., Mandal, S.K., Srivastava, L. and Buragohain, M.K. (2018a), "Flexural strength of delaminated composite plate-An experimental validation", *Int. J. Damage Mech.*, **27**(2), 296-329. https://doi.org/10.1177/1056789516676515.

Hirwani, C.K., Panda, S.K., Mahapatra, T.R., Mandal, S.K., Mahapatra, S.S. and De, A.K. (2018b), "Delamination effect on flexuralresponses of layered curved shallow shell panel-experimental and numerical analysis", *Int. J. Comput. Meth.*, **15**(4), 1850027. https://doi.org/10.1142/S0219876218500275.

Hirwani, C.K., Patil, R.K., Panda, S.K., Mahapatra, S.S., Mandal, S.K., Srivastava, L. and Buragohain, M.K. (2016a), "Experimental and numerical analysis of free vibration of delaminated curved panel", *Aerosp. Sci. Technol.*, **54**, 353-370. https://doi.org/10.1016/j.ast.2016.05.009.

Hirwani, C.K., Sahoo, S.S. and Panda, S.K. (2016b), "Effect of delamination on vibration behaviour of woven Glass/Epoxy composite plate-An experimental study", *IOP Conf. Ser.: Mater. Sci. Eng.*, **115**(1), 012010. https://doi.org/10.1088/1757-899X/115/1/012010.

Jha, D., Kant, T. and Singh, R. (2013), "Free vibration response of functionally graded thick plates with shear and normal deformations effects", *Compos. Struct.*, **96**, 799-823. https://doi.org/10.1016/j.compstruct.2012.09.034.

Jin, G., Su, Z., Shi, S., Ye, T. and Gao, S. (2014), "Three-dimensional exact solution for the free vibration of arbitrarily thick functionally graded rectangular plates with general boundary conditions", *Compos. Struct.*, **108**, 565-577. https://doi.org/10.1016/j.compstruct.2013.09.051.

Kar, V.R. and Panda, S.K. (2015), "Nonlinear flexural vibration of shear deformable functionally graded spherical shell panel",

Steel Compos. Struct., **18**(3), 693-709. https://doi.org/10.12989/scs.2015.18.3.693.

Kar, V.R. and Panda, S.K. (2016), "Nonlinear thermomechanical behavior of functionally graded material cylindrical/hyperbolic/elliptical shell panel with temperature-dependent and temperature-independent properties", *J. Press. Ves. Technol.*, **138**(6), 061202. https://doi.org/10.1115/1.4033701.

Karami, B. and Janghorban, M. (2019), "A new size-dependent shear deformation theory for free vibration analysis of functionally graded/anisotropic nanobeams", *Thin Wall. Struct.*, **143**, 106-227. https://doi.org/10.1016/j.tws.2019.106227

Keikha, R., Heidari, A., Hosseinabadi, H. and Haghighi, M.S. (2018), "Classical shell theory for instability analysis of concrete pipes conveying nanofluid", *Comput. Concrete*, **22**(2), 161-166. https://doi.org/10.12989/cac.2018.22.2.161.

Kerr, A.D. (1964), "Elastic and viscoelastic foundation models", *J. Appl. Mech.*, **31**(3), 491-498. https://doi.org/10.1115/1.3629667.

Kunche, M.C., Mishra, P.K., Nallala, H.B., Hirwani, C.K., Katariya, P.V., Panda, S. and Panda, S.K. (2019), "Theoretical and experimental modal responses of adhesive bonded T-joints", *Wind Struct.*, **29**(5), 361-369. https://doi.org/10.12989/was.2019.29.5.361.

Laoufi, I., Ameur, A., Zidi, M., Adda Bedia, E.A. and Bousahla, A.A. (2016), "Mechanical and hygro-thermal behaviour of functionally graded plates using a hyperbolic shear deformation theory", *Steel Compos. Struct.*, **20**(4), 889-912. https://doi.org/10.12989/scs.2016.20.4.889.

Liu, Y. (2011), "A refined shear deformation plate theory", *Int. J. Comput. Meth. Eng. Sci. Mech.*, **12**(3), 141-149.

Mantari, J., Granados, E., Hinostroza, M. and Soares, C.G. (2014), "Modelling advanced composite plates resting on elastic foundation by using a quasi-3D hybrid type HSDT", *Compos. Struct.*, **118**, 455-471. https://doi.org/10.1016/j.compstruct.2014.07.039.

Mantari, J.L, Oktem, A.S. and Soares, O.G. (2012), "Bending response of functionally graded plates by using a new higher order shear deformation theory", *Compos. Struct.*, **94**, 714-723. https://doi.org/10.1016/j.compstruct.2011.09.007.

Mehar, K. and Panda, S.K. (2018), "Elastic bending and stress analysis of carbon nanotube-reinforced composite plate: Experimental, numerical, and simulation", *Adv. Polym. Technol.*, **37**(6), 1643-1657. https://doi.org/10.1002/adv.21821.

Mehar, K. and Panda, S.K. (2019), "Theoretical deflection analysis of multi-walled carbon nanotube reinforced sandwich panel and experimental verification", *Compos. Part B: Eng.*, **167**, 317-328. https://doi.org/10.1016/j.compositesb.2018.12.058.

Mehar, K., Panda, S.K. and Mahapatra, T.R. (2017), "Theoretical and experimental investigation of vibration characteristic of carbon nanotube reinforced polymer composite structure", *Int. J. Mech. Sci.*, **133**, 319-329. https://doi.org/10.1016/j.ijmecsci.2017.08.057.

Mehar, K., Panda, S.K. and Mahapatra, T.R. (2019), "Large deformation bending responses of nanotube-reinforced polymer composite panel structure: Numerical and experimental analyses", *Proc. Inst. Mech. Eng., Part G: J. Aerosp. Eng.*, **233**(5), 1695-1704. https://doi.org/10.1177/0954410018761192.

Mindlin, R.D. (1951), "Thickness-shear and flexural vibrations of crystal plates", *J. Appl. Phys.*, **22**(3), 316-323. https://doi.org/10.1063/1.1699948.

Moradi-Dastjerdi, R. (2016), "Wave propagation in functionally graded composite cylinders reinforced by aggregated carbon nanotube". *Struct. Eng. Mech.*, **57**(3), 441-456. https://doi.org/10.12989/sem.2016.57.3.441.

Neves, A.M.A., Ferreira, A.J.M., Carrera, E., Cinefra, M., Roque, C.M.C., Jorge, R.M.N. and Soares, C.M. (2013), "Static, free vibration and buckling analysis of isotropic and sandwich functionally graded plates using a quasi-3D higher-order shear

deformation theory and a meshless technique", *Compos. Part B: Eng.*, **44**(1), 657-674. https://doi.org/10.1016/j.compositesb.2012.01.089.

Neves, A.M.A., Ferreira, A.J.M., Carrera, E., Roque, C.M.C., Cinefra, M., Jorge, R.M.N. and Soares, C.M.M. (2012), "A quasi-3D sinusoidal shear deformation theory for the static and free vibration analysis of functionally graded plates", *Compos. Part B: Eng.*, **43**(2), 711-725. https://doi.org/10.1016/j.compositesb.2011.08.009.

Neves, A.M.A., Ferreira, A.J.M., Carrera, E., Roque, C.M.C., Cinefra, M., Jorge, R.M.N. Soares, C.M.M. (2012). "A quasi-3D sinusoidal shear deformation theory for the static and free vibration analysis of functionally graded plates", *Compos. Part B.*, **43**, 711-725. https://doi.org/10.1016/j.compositesb.2011.08.009.

Nguyen, V.H., Nguyen, T.K., Tai, H.T. and Vo, T.P. (2014), "A new inverse trigonometric shear deformation theory for isotropic and functionally graded sandwich plates", *Compos. B*, **66**, 233-246. https://doi.org/10.1016/j.compositesb.2014.05.012.

Pandey, H.K., Hirwani, C.K., Sharma, N., Katariya, P.V. and Panda, S.K. (2019), "Effect of nano glass cenosphere filler on hybrid composite eigenfrequency responses - An FEM approach and experimental verification", *Adv. Nano Res.*, **7**(6), 419-429. https://doi.org/10.12989/anr.2019.7.6.419.

Pasternak, P. (1954), "On a new method of analysis of an elastic foundation by means of two foundation constants", *Gosudarstvennoe Izdatelstvo Literaturipo Stroitelstvu i Arkhitekture*, Moscow.

Pradhan, K.K. and Chakraverty, S. (2015), "Free vibration of functionally graded thin elliptic plates with various edge supports", *Struct. Eng. Mech.*, **53**(2), 337-354. https://doi.org/10.12989/sem.2015.53.2.337.

Qian, L.F. and Batra, R.C. (2005), "Three-dimensional transient heat conduction in a functionally graded thick plate with a higher-order plate theory and a meshless local Petrov-Galerkin Method", *Comput. Mech.*, **35**(3), 214-226. https://doi.org/10.1007/s00466-004-0617-6.

Rajabi, J. and Mohammadimehr, M. (2019), "Bending analysis of a micro sandwich skew plate using extended Kantorovich method based on Eshelby-Mori-Tanaka approach", *Comput. Concrete*, **23**(5), 361-376. https://doi.org/10.12989/cac.2019.23.5.361.

Reissner, E. (1945), "The effect of transverse shear deformation on the bending of elastic plates", *J. Appl. Mech.*, A69-A77.

Sahoo, S.S., Hirwani, C.K., Panda, S.K. and Sen, D. (2018), "Numerical analysis of vibration and transient behaviour of laminated composite curved shallow shell structure: An experimental validation", *Scientia Iranica*, **25**(4), 2218-2232.

Sahoo, S.S., Panda, S.K. and Singh, V.K. (2017a), "Experimental and numerical investigation of static and free vibration responses of woven glass/epoxy laminated composite plate", *Proc. Inst. Mech. Eng. Part L: J. Mater.: Des. Appl.*, **231**(5), 463-478. https://doi.org/10.1177/1464420715600191.

Sahoo, S.S., Panda, S.K., Mahapatra T.R. and Hirwani, C.K. (2019), "Numerical analysis of transient responses of delaminated layered structure using different mid-plane theories and experimental validation", *Iran. J. Sci. Technol. Tran. Mech. Eng.*, **43**(1), 41-56. https://doi.org/10.1007/s40997-017-0111-3.

Sahoo, S.S., Panda, S.K., Singh, V.K. and Mahapatra T.R. (2017b), "Numerical investigation on the nonlinear flexural behaviour of wrapped glass/epoxy laminated composite panel and experimental validation", *Arch. Appl. Mech.*, **87**, 315-333. https://doi.org/10.1007/s00419-016-1195-8.

Sahoo, S.S., Singh, V.K. and Panda, S.K. (2016), "Nonlinear flexural analysis of shallow carbon/epoxy laminated composite curved panels: experimental and numerical investigation", *J. Eng. Mech.*, **142**(4), 04016008. https://doi.org/10.1061/(ASCE)EM.1943-7889.0001040.

Salari, E., Ashoori, A. and Vanini, S.A.S. (2019), "Porosity-dependent asymmetric thermal buckling of inhomogeneous annular nanoplates resting on elastic substrate", *Adv. Nano Res.*, **7**(1), 25-38. https://doi.org/10.12989/anr.2019.7.1.025.

Shahsavari, D., Shahsavari, M., Li, L. and Karami, B. (2018), "A novel quasi-3D hyperbolic theory for free vibration of FG plates with porosities resting on Winkler/Pasternak/Kerr foundation", *Aerosp. Sci. Technol.*, **72**, 134-149. https://doi.org/10.1016/j.ast.2017.11.004.

Shimpi, R.P., Arya, H. and Naik, N.K. (2003), "A higher order displacement model for the plate analysis", *J. Reinf. Plast. Compos.*, **22**(22), 1667-1688. https://doi.org/10.1177/073168403027618.

Srinivas, S., Joga, C.V. and Rao, A.K. (1970), "Bending, vibration and buckling of simply supported thick orthotropic rectangular plate and laminates", *Int. J. Solid. Struct.*, **6**, 1463-1481. https://doi.org/10.1016/0020-7683(70)90076-4.

Thai, H.T. and Choi, D.H. (2011), "A refined plate theory for functionally graded plates resting on elastic foundation", *Compos. Sci. Technol.*, **71**(16), 1850-1858. https://doi.org/10.1016/j.compscitech.2011.08.016.

Thai, H.T. and Kim, S.E. (2013), "A simple higher order shear deformation theory for bending and free vibration of functionally graded plates", *Compos. Struct.*, **96**, 165-173. https://doi.org/10.1016/j.compstruct.2012.08.025.

Thai, H.T. and Kim, S.E. (2013), "A simple quasi-3D sinusoidal shear deformation theory for functionally graded plates", *Compos. Struct.*, **99**, 172-180. https://doi.org/10.1016/j.compstruct.2012.11.030.

Thai, H.T., Vo, T.P., Bui, T.Q. and Nguyen, T.K. (2014), "A quasi-3D hyperbolic shear deformation theory for functionally graded plates", *Acta Mechanica*, **225**(3), 951-964. https://doi.org/10.1007/s00707-013-0994-z.

Wu, C.P. and Chiu, K.H. (2011), "RMVT-based meshless collocation and element- free Galerkin methods for the quasi-3D free analysis of multilayed composite and FGM plates", *Compos. Struct.*, **93**(5), 1433-1448. https://doi.org/10.1016/j.compstruct.2010.07.001.

Zenkour, A.M. (2006), "Generalized shear deformation theory for bending analysis of functionally graded material", *Appl. Math. Model.*, **30**, 67-84. https://doi.org/10.1016/j.apm.2005.03.009.

Zenkour, A.M. (2018), "A quasi-3D refined theory for functionally graded single-layered and sandwich plates with porosities", *Compos. Struct.*, **201**, 38-48. https://doi.org/10.1016/j.compstruct.2018.05.147.

Zenkour, A.M. (2019), "Quasi-3D refined theory functionally graded porous plates: Displacements and stresses", *Appl. Math. Model.* **22**(1), 22-35. https://doi.org/10.24411/1683-805X-2019-11003.

Zenkour, A.M. and Sobhy, M. (2013), "Dynamic bending response of thermoelastic functionally graded plates resting on elastic foundations", *Aerosp. Sci. Technol.*, **29**(1), 7-17. https://doi.org/10.1016/j.ast.2013.01.003.

Zhou, D., Cheung, Y., Au, F. and Lo, S. (2002), "Three-dimensional vibration analysis of thick rectangular plates using Chebyshev polynomial and Ritz method", *Int. J. Solid. Struct.*, **39**, 6339-6353. https://doi.org/10.1016/S0020-7683(02)00460-2.

CC